Accepted Article

PROF. JUN GUO (Orcid ID : 0000-0002-5552-734X)

Article type : MS - Regular Manuscript

Jun Guo ORCID iDs: 0000-0002-6000-2556

A stripe rust effector Pst18363 targets and stabilizes TaNUDX23 that promotes stripe rust disease

Qian Yang, Baoyu Huai, Yuxi Lu, Kunyan Cai, Jia Guo, Xiaoguo Zhu, Zhensheng Kang* and Jun Guo*

State Key Laboratory of Crop Stress Biology for Arid Areas, College of Plant Protection, Northwest A&F University, Yangling 712100, Shaanxi, P. R. China

***Authors for correspondence:**

Jun Guo, Tel: +86 29 87082439, E-mail: guojunwgq@nwsuaf.edu.cn.

Zhensheng Kang, Tel: +86 29 87080061, E-mail: kangzs@nwsuaf.edu.cn.

Received: 10 March 2019

Accepted: 9 September 2019

This article has been accepted for publication and undergone full peer review but has not been through the copyediting, typesetting, pagination and proofreading process, which may lead to differences between this version and the Version of Record. Please cite this article as doi: 10.1111/NPH.16199

This article is protected by copyright. All rights reserved

Word Count:

Total words: 6481, Summary: 187, Introduction: 812, Materials and Methods: 1781, Results: 2870, Discussion: 985, Acknowledgement: 33.

Number of Figures: 8 (color: 8)

Number of Tables: 0

Supporting Information: Twelve Figures (S1-S12); Four Tables (Table S1-S4).

Accepted Article

This article is protected by copyright. All rights reserved

Accepted Article

Summary

- Wheat stripe rust, caused by *Puccinia striiformis* f. sp. *tritici* (*Pst*), poses a tremendous threat to the production of wheat worldwide. Molecular mechanisms of *Pst* effectors regulating wheat immunity are poorly understood.
- In this study, we identified an effector Pst18363 from *Pst* which suppresses plant cell death in *Nicotiana benthamiana* and in wheat. Knocking down *Pst18363* expression by virus-mediated host-induced gene silencing (HIGS) significantly decreased the number of rust pustules, indicating that *Pst18363* functions as an important pathogenicity factor in *Pst*.
- Pst18363 was proven to interact with wheat Nudix hydrolase 23 TaNUDX23. In wheat, silencing of *TaNUDX23* by virus-induced gene silencing (VIGS) increased reactive oxygen species (ROS) accumulation induced by the avirulent *Pst* race CYR23, whereas overexpression of *TaNUDX23* suppressed reactive oxygen species (ROS) accumulation induced by flg22 in *Arabidopsis*. In addition, TaNUDX23 suppressed *Pst* candidate effector Pst322-trigged cell death by decreasing ROS accumulation in *N. benthamiana*. Knocking down of *TaNUDX23* expression attenuated *Pst* infection, indicating that TaNUDX23 is a negative regulator of defense. In *N. benthamiana,* Pst18363 stabilizes TaNUDX23.
- Overall, our data suggest that Pst18363 stabilizes TaNUDX23, which suppresses ROS accumulation to facilitate *Pst* infection.

Key words: *Puccinia striiformis* f. sp. *tritici*, effector, wheat (*Triticum aestivum*), Nudix hydrolase, reactive oxygen species (ROS).

This article is protected by copyright. All rights reserved

Accepted Article

Introduction

Because plants grow in an environment surrounded by diverse pathogens and their lack of ability to escape pathogens, plants have developed sophisticated defense strategies against pathogens for survival. Upon pathogen infection, the first level of defense, which is frequently referred to as PAMP-triggered immunity (PTI), is initiated by the recognition of pathogen-associated molecular patterns (PAMPs) by pattern recognition receptors (PRRs) to prevent further colonization by the pathogen (Jones & Dangl, 2006). In addition to PTI, the second layer of defense called effector-triggered immunity (ETI) evolved to protect the host from further invasion in the interaction between plants and pathogens (Chisholm *et al.*, 2006). However, pathogens have evolved mechanisms to manipulate the signaling processes of PTI or ETI by delivering secreted proteins (effectors) inside living plant cells to target host proteins, allowing successful colonization and infection (Jones & Dangl, 2006). Therefore, identifying and characterizing host proteins targeted by pathogen effectors will provide deeper insights into the mechanisms of effector activity and into the host processes that are targeted.

In recent years, studies to characterize the function of host proteins targeted by effectors from bacteria and oomycetes have contributed notable achievements, which showed that effectors regulate the host immune system by interacting with host proteins. For instance, the *Pseudomonas syringae* type III effectors, including HopAI1 and HopF2, directly attack components of MAPK cascades to inhibit PTI signaling (Zhang *et al.*, 2007; Wang *et al.*, 2010). *Phytophthora capsici* deploys an RXLR effector, PcAvr3a12, to facilitate infection by targeting and suppressing a novel ER-localized PPIase, FKBP15-2, which is required for ER stress-mediated plant immunity (Fan *et al.*, 2018). However, relatively little is known about the host targets of effectors from obligate biotrophic pathogens, such as rust fungi.

A member of a large family of rust fungi*, Puccinia striiformis* f. sp. *tritici* (*Pst*) is the causative agent of stripe rust, the most widespread and devastating disease of wheat,

This article is protected by copyright. All rights reserved

which resulted in yield losses of more than 90% in a single crop season (Line, 2002; Wellings, 2011; Chen, 2014). The obligate biotrophy and the lack of a transformation system for *Pst* complicates validation of the function of effectors from *Pst* and their host targets. To date, five effectors from *Pst* have been identified. However, thus far, only two secreted effectors of *Pst* have been confirmed to interact with host targets, adenosine kinases and NPR1, respectively (Wang *et al.*, 2016; Liu *et al.*, 2017). Therefore, to better reveal the pathogenic mechanism of *Pst* during infection, there is an urgent need to fill the vacancy by identifying *Pst* effector proteins and host processes that are targeted by these effectors.

Nudix hydrolases are a family of pyrophosphohydrolases which contain a conserverd Nudix domain GX5EX7REVXEEXGU, where U is usually Leu, Ile or Val and X is any amino acid. The family is widespread among bacteria, archaea, viruses and eukaryotes (Bessman *et al.*, 1996; Dunn *et al.*, 1999). Nudix hydrolases hydrolyze a wide range of substrates such as pyridine nucleotides, nucleotide sugars, coenzyme A, capped RNA, and oxidized nucleoside di- and triphosphates (McLennan, 2006; Gunawardana *et al.*, 2009). Some of these substrates are cell signaling molecules, whereas others are potentially toxic compounds or coenzymes. Thus, Nudix hydrolases are considered to play a key role in regulating, protecting and signaling by modulating the levels of their substrates. In *Arabidopsis thaliana*, 29 Nudix hydrolase genes have been identified (Kraszewska, 2008). Among these genes, AtNUDX7 has been identified as a gene induced by multiple stresses. In *A. thaliana*, knockout of AtNUDX7 (KO-nudx7) leads to constitutive expression of pathogenesis-related genes, disruption of cellular redox homeostasis and accumulation of salicylic acid (SA), and thereby enhances resistance to *P. syringae* and *Hyaloperonospora arabidopsidis* (Ge *et al.*, 2007; Bartsch *et al.*, 2006). These results indicate that AtNUDX7 acts as a negative regulator in disease resistance pathways. Interestingly, Nudix proteins have been identified as secreted effectors in some pathogens. Protein Hpx26 secreted by *Ralstonia solanacearum* shares homology with a known Nudix hydrolase (Tamura *et al.*, 2005). In addition, *Phytophthora sojae* avirulence

This article is protected by copyright. All rights reserved

effector Avr3b with a Nudix domain possesses the ADP-ribose/NADH pyrophosphorylase activity, and overexpression of *Avr3b* in *N. benthamiana* increases susceptibility to *Phytophthora* and suppresses the accumulation of ROS around infection sites (Dong *et al.*, 2011). These previous discoveries suggest that pathogens can utilize the Nudix hydrolase activity to promote infection by secreting effector proteins with a Nudix motif. However, whether pathogens can directly secrete effectors to target host Nudix hydrolase for increasing infection during the plant-pathogen interactions remains unknown.

In this study, we identified wheat nucleoside diphosphate hydrolase TaNUDX23 as a target of a *Pst* effector, PSTCY32_18363 (alias Pst18363) that is an ortholog of rust transferred protein 1 (Uf-RTP1) from *Uromyces fabae* (Kemen *et al.*, 2005; Kemen *et al.*, 2013; Pretsch *et al.*, 2013) and required for full virulence of *Pst* in wheat. Further analyses showed that Pst18363 stabilizes TaNUDX23, which suppresses ROS accumulation and facilitates *Pst* infection.

Materials and Methods

Plant materials and fungal strains

Wheat cultivar Suwon11 (Su11) and *N. benthamiana* were used in this study. Wheat cultivar Su11, which is highly susceptible to CYR31 and CYR32 and highly resistant to CYR23, was used for analysis of gene transcription levels and for HIGS or VIGS assays. Wheat seedlings were cultivated, inoculated with *Pst* and maintained according to procedures and conditions described previously (Kang *et al.*, 2002). *N. benthamiana* seedlings in the four-leaf stage were infiltrated with *Agrobacterium tumefaciens* GV3101 for bimolecular fluorescence complementation (BIFC) and co-immunoprecipitation (CoIP) assays. *A. thaliana* used in this study includes wild-type (WT) and TaNUDX23 over-expression plants.

Pst isolates CYR23, CYR31 and CYR32 were used for infection. Fresh urediospores were collected from the infected leaves of Su11 that were grown at 16 °C in artificial

This article is protected by copyright. All rights reserved

climate chamber.

RT-PCR Analysis

To assay transcript levels of *Pst18363*, urediospores and leaves of wheat Su11 infected with CYR32 at 6, 12, 18, 24, 48, 72, 120, 168, and 264 h post-inoculation (hpi) were harvested. To analyze the transcript levels of *TaNUDX23*, leaves of Su11 inoculated with CYR31 at 0, 12, 24, 48, 72, 120 hpi were sampled. RNA of all samples was extracted with the Quick RNA isolation Kit (Huayueyang Biotechnology, China, Beijing). Approximately 2 μg of the total RNA were also used for reverse transcription using RevertAid First Strand cDNA Synthesis Kit (MNI, K1622). qRT-PCR on a CFX Connect Real-Time System (Bio-Rad, Hercules, CA, USA) was performed in a 25-μl reaction mixture containing 12.5 μl of LightCycler SYBR Green I Master Mix, 2 μl of diluted cDNA (1:5), 8.9 μl of distilled H_2O, 0.8 μl of forward primer (10 mM) and 0.8 μl of reverse primer (10 mM). The primers used are listed in Supporting Information Table S1. Real-time PCR data were analyzed by the comparative $2^{-\Delta\Delta CT}$ method to quantify relative gene expression (Livak & Schmittgen, 2001). The transcript levels of *Pst18363* and *TaNUDX23* were normalized to *PstEF-1* and *TaEF-1*, respectively. Each sample was analyzed in three biological replications, and each PCR analysis included three technical repeats. The statistical significance was evaluated by Student's t-test.

Yeast Signal Sequence Trap System

To validate the function of the predicted signal peptide of Pst18363, the yeast signal sequence trap system was used as described previously (Yin *et al.*, 2018). The predicted signal peptide sequence of Pst18363 was cloned into vector pSUC2T7M13ORI (pSUC2) using the specific primers (Table S1) and then was transformed into the invertase mutant yeast strain YTK12 (Oh *et al.*, 2009). CMD-W medium (0.67% yeast N base without amino acids, 0.075% W dropout supplement, 2% sucrose, 0.1% glucose, and 2% agar) was used for screening the positive colonies. The secretory function was confirmed by growth

This article is protected by copyright. All rights reserved

on YPRAA plates (1% yeast extract, 2% peptone, 2% raffinose, and 2 μg ml^{-1} antimicyn A) containing raffinose and lacking glucose. Moreover, invertase enzymatic activity was detected by the reduction of 2,3,5-Triphenyltetrazolium Chloride (TTC) to insoluble red colored 1,3,5-triphenylformazan (TPF) according to procedures and conditions described previously (Jacobs *et al.*, 1997).

A. tumefaciens Infiltration Assays

To assay suppression of BAX- or Pst322-triggered cell death by effector Pst18363, the *A. tumefaciens*-mediated transient expression method was used. The sequence encoding *Pst18363* without the signal peptide (Pst18363(ΔSP)) was amplified with primers Pst18363-HA-F/R (Table S1), and introduced into vector pGR106 to construct PVX-Pst18363-HA plasmid. Resuspended *Agrobacterium* cultures carrying eGFP or Pst18363-HA at a final OD600 of 0.2 and 10 mM $MgCl_2$ buffer were infiltrated into *N. benthamiana* leaves (Bos *et al.*, 2006). The infiltration sites were challenged 24 h later with recombinant *A. tumefaciens* carrying BAX or Pst322 at a final OD600 of 0.2. The infiltrated *N. benthamiana* plants were kept in a greenhouse with high light intensity at 25 °C. Expression of genes in all infiltration sites were detected by RT-PCR and immunoblot three days after infiltration. Symptoms were monitored and recorded from 6 to 8 days after infiltration. Three independent biological replicates were conducted for each experiment.

Yeast-Two-Hybrid assay (Y2H)

A *Pst* cDNA library was generated with total RNA extracted from CYR32-infected wheat leaves. For screening the library, Pst18363(ΔSP) was amplified with primers Pst18363-BD-F/R (Table S1) and cloned into pGBKT7 to create the BD-Pst18363 vector. For Y2H, the BD-Pst18363 vector, acting as a bait, was transformed into yeast strain AH109. The single positive yeast AH109 clone was used to prepare competent yeast cells, which were transformed with the above mentioned Y2H 'prey' library, and the yeast cell

This article is protected by copyright. All rights reserved

suspension containing BD-Pst18363 and cDNA library was placed on SD/-Trp-Leu and SD/-Trp-Leu-His selection medium. For further selection, we picked colonies from SD/-Trp-Leu-His medium to plate on SD/-Trp-Leu-His-Ade medium. Subsequently, we analyzed the sequences of colonies from SD/-Trp-Leu-His-Ade medium by BLASTn using the NCBI database. To confirm the interaction target of Pst18363, the full-length cDNA of each candidate target was cloned into pGADT7 vector and transformed into yeast strain AH109 containing the vector BD-Pst18363. The interactions were confirmed by growth on the SD/-Trp-Leu-His-Ade medium containing X-α-gal.

GST Pull-Down Assay

The GST Protein Interaction Pull-Down Kit (Thermo Scientific, cat. no. TA260524) was used for pull-down assay of Pst18363 and TaNUDX23. To construct His-Pst18363 and GST-TaNUDX23, Pst18363(ΔSP) were cloned into the pET-32a(+) vector and TaNUDX23 was cloned into pGEX-4T-1 vector with specific primers (Table S1). Vectors were transformed into *E. coli* BL21 cells for protein expression. The pull-down assay was performed according to the manufacturer's instructions. HRP conjugated anti GST-Tag rabbit polyclonal antibody (Cwbiotech, cat. no. CW0144M) and HRP conjugated anti His-Tag mouse monoclonal antibody (Cwbiotech, cat. no. CW0285M) were used for the western blots.

BIFC Assays in *N. benthamiana*

For BIFC assays of Pst18363 and TaNUDX23, Pst18363(ΔSP) was cloned into pSPYNE and pSPYCE to make nYFP-Pst18363 and cYFP-Pst18363 constructs, and a full-length cDNA from TaNUDX23 was cloned into pSPYNE(R)173 and pSPYCE(M) to make nYFP-TaNUDX23 and cYFP-TaNUDX23 constructs (Table S1). *A. tumefaciens* carrying these constructs were infiltrated into 4-week-old *N. benthamiana* leaves in four combinations (pSPYNE with cYFP-Pst18363, nYFP-TaNUDX23 with pSPYCE, nYFP-TaNUDX23 with cYFP-Pst18363, nYFP-Pst18363 with cYFP-TaNUDX23) together

This article is protected by copyright. All rights reserved

with the p19 strain (Voinnet *et al.*, 2003). Confocal images were taken 48 h after agroinfiltration at 488 nm wavelength laser by an Olympus IX83 confocal microscope (Japan). BIFC assays of Pst18363 and other TaNUDX protein or candidate targets were performed according to the above procedure.

CoIP Assays

CoIP assays were performed by transient expression in *N. benthamiana* leaves. A full-length cDNA from TaNUDX23 was amplified and inserted into the vector pBI121 mutant, in which reporter gene GUS was replaced with red fluorescence gene mCherry, to make mCherry-TaNUDX23 construct using primers TaNUDX23-mCherry-F/R (Table S1). To make Pst18363-YFP construct, Pst18363(ΔSP) was amplified and ligated into binary vector pBamEYFP. The *Agrobacterium* strain carrying the vector YFP-Pst18363 or eYFP (pBamEYFP) was mixed with *Agrobacterium* strain containing the vector mCherry-TaNUDX23 in a ratio 1:1, and then infiltrated into *N. benthamiana* leaves. At 48 h after agroinfiltration, total protein was extracted with extraction buffer (50 mM Tris pH 7.5, 150 mM NaCl, 1% NP-40, 5 mM DTT, protease inhibitor cocktail Complete Mini tablets [Roche]). For CoIP assays, 10 µl GFP-Trap agarose beads (Chromotek), which were washed at least four times with the extraction buffer beforehand, were incubated with 2 ml of crude protein at 4 °C for 3 h with gentle shaking (Win *et al.*, 2011). The precipitated proteins were washed five times with PBS buffer. The precipitated proteins and crude proteins (input) were detected by immunoblotting with anti-GFP antibody (Sungene Biotech, KM8009) and anti-mCherry antibody (Sungene Biotech, KM8017).

Activity Assays of T**aNUDX23**

The assays were carried out in a 50 µl hydrolysis mixture containing 50 mM Tris-HCl (pH 8.5), 5 mM MgCl2, 1 mM dithiothreitol, 2 mM substrate, 2 units of calf alkaline phosphatase, 5 µg of protein samples. After incubation for 30 min at 37 °C, the reaction was stopped by addition of 150 µl of 1N H_2SO_4, followed by addition of 100 µl of water and

This article is protected by copyright. All rights reserved

700 µl of a freshly prepared mixture containing 600 µl of 0.42% molybdate·$4H_2O$ and 100 µl of 10% ascorbic acid. The reaction tubes were incubated in a 45 °C water bath for 20 min for color development and then cooled to room temperature. The reaction with GST was used as a negative control for each substrate. To investigate effects of Ca^{2+} on TaNUDX23 activity, $CaCl_2$ was added to the hydrolysis mixture to a concentration of 7 mM. All the substrates were purchased from Sigma.

Oxidative Burst measurement

First, we cloned TaNUDX23 into a binary vector pK7WGR2 via LR gateway methods to construct Pk7-TaNUDX23 vector using primers TaNUDX23-Pk7-F/R (Table S1). *A. tumefaciens* carrying Pk7-TaNUDX23 vector was used to infect *Arabidopsis* for generating *TaNUDX23* over-expression plants as described previously (Xiao *et al.*, 2001). Leaves from 4-week-old WT and TaNUDX23 over-expression transgenic line 2 and line 5 T3 plants were sliced into 1 mm^2 discs, and maintained in water in a 96-well plate overnight. Then, the leaf discs were treated with 200 µl of solution containing 100 nM of the bacterial flagellar peptide flg22, 20 µg ml^{-1} peroxidase (Sigma-Aldrich) and 20 nM luminol. Luminescence was recorded for 60 min by using a multiscan spectrum. Each data point consists of six replicates. These experiments were repeated three times.

BSMV-mediated silencing

Two cDNA fragments of *Pst18363*, *Pst24948*, *Pst09949* or *TaNUDX23* were designed using Prime 5 and evaluated by BLASTn search in the NCBI database. BLASTn analysis showed that the two fragments were specific for silencing of these genes. The two fragments of these genes were cloned and inserted into barley stripe mosaic virus (BSMV) as previously described (Holzberg *et al.*, 2002), resulting in BSMV: Pst18363-1/2as, BSMV: Pst24948-1/2as, BSMV: Pst09949-1/2as, BSMV: TaNUDX23-1/2as (Table S1). These plasmids were linearized followed by transcribing and capping in vitro using the RiboMAX Large-Scale RNA Production System-T7 and the Ribom7G Cap Analog (both

This article is protected by copyright. All rights reserved

by Promega) following the manufacturer's instructions. The capped BSMV transcripts were then inoculated onto the second leaf of the two-leaf-stage wheat with 1 × FES buffer by rubbing with gloved fingers. BSMV: TaPDSas encoding the *T. aestivum* phytoene desaturase was used as positive control, whereas wheat seedlings inoculated with only 1 × FES buffer or BSMV: γ were used as negative control. The wheat seedlings infected with virus were maintained in controlled chamber at 25 ± 3 °C. Fourteen days after virus inoculation, the fourth leaves of wheat inoculated with virus were inoculated with fresh CYR32 urediospores (for silencing of *Pst18363*) or CYR23/31 (for silencing of *TaNUDX23*) and maintained at 16 °C. The fourth leaves were sampled at 24, 48, 120 hpi for assessment of silencing efficiency and histological observation. The phenotypes of the fourth leaves were photographed at 12 d after inoculation with *Pst*. Finally, the photographed leaves were collected to measure the biomass ratio by qRT-PCR (Liu *et al.*, 2016). These experiments were repeated three times.

Results

Identification of the Candidate Effector Pst18363

Genome analyses of Chinese *Pst* isolate CYR32 revealed a number of potential secreted proteins in *Pst* (Zheng *et al.*, 2013). Relatively few secreted proteins that function in suppressing host defense in *Pst* have been characterized. The ability to suppress programmed cell death (PCD) induced by the pro-apoptotic mouse protein BAX has proven to be a valuable initial screen for pathogen effectors capable of suppressing defense-associated PCD (Jamir *et al.*, 2004; Dou *et al.*, 2008). We performed a primary screen to identify candidate effectors that are capable of suppressing defense-associated PCD. A total of 30 effectors were randomly cloned into PVX vector pGR106. Using an *A. tumefaciens*–mediated transient expression assay in *N. benthamiana*, we infiltrated *Agrobacterium* strains carrying each effector into *N. benthamiana* leaves 24 h prior to infiltration of *Agrobacterium* strains carrying BAX. At 7 days, a candidate effector

This article is protected by copyright. All rights reserved

Accepted Article

Pst18363 (GenBank accession number MK614574) was shown to suppress BAX-triggered PCD compared with eGFP control (Fig. S1a, b).

Pst18363 has an open reading frame of 660 bp, encoding a protein of 220 amino acids without a known conserved domain. Phylogenetic analysis showed that Pst18363 is an ortholog of *Uromyces fabae* effector Uf-RTP1 (Kemen *et al.*, 2005; Kemen *et al.*, 2013; Pretsch *et al.*, 2013) (Fig. S2a; Table S2). Sequence analysis indicated that Pst18363, like other RTP1p homologs, contains seven highly conserved β strands and two aggregation domains in the C-terminal region starting at position 94 referring to the Uf-RTP1p sequence (Fig. S2b). SignalP 4.1 analysis showed that Pst18363 has a signal peptide encoded by the first 51 bp. To confirm the secretory function of the predicted signal peptide of Pst18363, we used a signal sequence trap system (Yin *et al.*, 2018). The pSUC2 vector fused with the signal peptide of oomycete effector Avr1b (Shan *et al.*, 2004) was used as a positive control, whereas the YTK12 strains with or without pSUC2 vector were used as negative controls. Only yeast YTK12 transformed with Pst18363 and Avr1b constructs grew on YPRAA medium (Fig.S3). In addition, to further confirm the secretory function of the signal peptide, we tested invertase enzymatic activity, in which secreted invertase reduced TTC to insoluble red colored TPF. We found that the TTC-treated Pst18363 and Avr1b culture filtrates turned red, whereas the negative control culture filtrates treated with TTC remained colorless (Fig. S3). These results indicate that the signal peptide of Pst18363 is functional.

Transcript level of *Pst18363* is up-regulated during the early infection stages and "sporulation" stage

In order to characterize the expression pattern of *Pst18363* during *Pst* infection stages, we analyzed its relative transcription levels by qRT-PCR at different time points during the infection process. *Pst18363* transcripts were detected in fresh ungerminated urediospores of CYR32 and in infected wheat samples collected from 6 to 264 hpi. RT-PCR assays showed that the transcription levels of *Pst18363* is up-regulated at the early stages of *Pst*

This article is protected by copyright. All rights reserved

CYR32 infection (6, 12, 18, 24, 48 hpi), and induced a higher transcription level (approximately 15-fold) at 24 hpi, which corresponds to the formation of haustorium (Fig. 1). The transcript levels were down-regulated at the late "parasitic/biotroph" stage (72-168 hpi). In addition, the expression of this gene was induced 7-fold at the "sporulation" stage (Fig. 1). Transcript profiles of *Pst18363* during the infection process suggest a putative function of *Pst18363* in *Pst* infection.

Silencing *Pst18363* reduces pathogenicity of *Pst*

To test whether Pst18363 is involved in *Pst* pathogenicity, host-induced gene silencing (HIGS) mediated by BSMV was used to silence *Pst18363* expression in *Pst* during the infection process. Two approximately 250-bp silencing fragments of *Pst18363* were designed to generate two different BSMV constructs for specifically silencing *Pst18363.* Pst09949, a homolog of *Ustilago maydis* CYP51 (XP_011390148.1), was used as positive control. Pst24948 which is homologous to Pst18363 and has been previously proved to be irresponsible for the pathogenicity of *Pst*, was used as negative control (Table S3). All of the wheat leaves infected with BSMV: γ, BSMV: Pst18363-1/2as, BSMV: Pst24948-1/2as and BSMV: Pst09949-1/2as expressed similar phenotypes of mild chlorotic mosaic symptoms at 12 dpi (Fig. 2a). Obvious photo-bleaching was observed in the BSMV: TaPDS-inoculated wheat, indicating that the BSMV-HIGS system functioned effectively (Fig. 2a). Subsequently, the fourth leaves of BSMV-inoculated wheat were inoculated with fresh ungerminated urediospores of CYR32. The number of rust pustules was significantly reduced in the wheat leaves inoculated with BSMV: Pst18363-1/2as and BSMV: Pst09949-1/2as compared with the leaves of BSMV: Pst24948-1/2as- and BSMV: γ-inoculated wheat (Fig. 2b). qRT-PCR analysis of total RNA extracted from silenced leaves, which were sampled at 120 hpi, revealed that the expression of *Pst18363, Pst09949* and *Pst24948* was significantly reduced (Fig. 2c). The relative *Pst* biomass also showed a decrease in the leaves inoculated with BSMV: Pst18363 and BSMV: Pst09949 compared with negative controls BSMV: γ and BSMV: Pst24948 (Fig. 2d). In addition,

This article is protected by copyright. All rights reserved

histological analysis by fluorescence microscope revealed that initial haustorium formation and growth of secondary hyphae were both reduced in BMSV: Pst18363-1/2as infected plants (Fig. S4). These results indicate that *Pst18363* contributes to pathogenicity of *Pst* on wheat leaves.

Pst18363 suppresses cell death in tobacco and wheat

To explore the mechanisms by which Pst18363 contributes to pathogenicity, we investigated whether, like other bacterial and fungal effectors, Pst18363 could suppress plant cell death. In this study, we chose the *Pst* candidate effector Pst322 as a trigger for cell death (Wang *et al.*, 2012), and *A. tumefaciens*-mediated transient expression method in *N. benthamiana* was used. The leaves were infiltrated with 10 mM $MgCl_2$ buffer or with *A. tumefaciens* cells containing Pst18363-HA or GFP 24 h prior to infiltration with *A. tumefaciens* cells carrying Pst322. At 5 days after the last infiltration, no cell death symptoms were observed in regions of the leaf pre-infiltrated with *A. tumefaciens* carrying Pst18363-HA, whereas Pst322-induced cell death symptoms were evident in regions pre-infiltrated with buffer or *A. tumefaciens* carrying GFP (Fig. 3a). As expected, infiltration with buffer, *A. tumefaciens* carrying Pst18363-HA, or GFP alone did not elicit visible cell death (Fig. 3a). Furthermore, the necrosis index of infiltrated regions showed that the necrosis ratio of the regions co-infiltrated with *A. tumefaciens* carrying Pst18363-HA and Pst322-Flag were almost the same as that of the regions without infiltration of *A. tumefaciens* carrying Pst322 (Fig. 3b). In addition, RT-PCR analysis (Fig. 3c) and western blotting (Fig. 3d) confirmed the normal expression of genes (GFP, Pst18363-HA and Pst322) in the infiltrated regions.

To further confirm that Pst18363 could suppress Pst322-triggered PCD, a particle bombardment assay was performed to introduce DNA encoding β-glucuronidase (GUS) into wheat leaves using a Bio-Rad Gene Gun (Wang *et al.*, 2012). The number of GUS-positive blue patches in the wheat leaves co-bombarded with Pst322 and Pst18363 were significantly more compared directly to that in the wheat leaves co-bombarded with

This article is protected by copyright. All rights reserved

Pst322 and empty vector (Fig. 3e, f). These results support the conclusion that Pst18363 can suppress PCD triggered by Pst322 in plant cells.

Pst18363 interacts with TaNUDX23 *in vitro* and *in vivo*

To understand the potential virulence function of Pst18363 in wheat, a yeast two-hybrid screen assay was performed to identify potential host targets of Pst18363. With Pst18363(ΔSP) as the bait, a total of 11 distinct, putative targets (Table S4), named Pst18363-interacting proteins Pst18363IPs, were isolated from a wheat cDNA library established from infected wheat with CYR32. Since the interaction between Ta10 and Pst18363 was the strongest in our preliminary screening experiment with BIFC assay (Fig. S5), we focused on the function of Ta10 in the subsequent studies. Ta10 was homologous to *Aegilops tauschii* Nudix hydrolase 23 protein (AetNUDX23, XP_020186566.1) containing a conserved Nudix domain. The sequence of *Ta10* was used to blast the hexaploid wheat genome databases (http://plants.ensembl.org/index.html), showing that two homologous sequences of *Ta10* were located on chromosomes 5A and 5B, respectively, and the homologous sequence of *Ta10* located on chromosome D was calibrated according to the sequence of *AetNUDX23* (Fig. S6a, b). Considering that the three homologous sequences are highly conserved in amino acid sequence (more than 99% identity; Fig. S6b), we used the sequence obtained from chromosome A here as a representative for all protein analyses, and named it as TaNUDX23 based on the phylogenetic analysis (Fig. S7a).

To confirm the preliminary Y2H results, Pst18363(ΔSP) was cloned into pGBKT7 vector as bait, and full-length *TaNUDX23* was cloned into pGADT7 vector as prey. Yeast colony growth on the selection medium SD/-Trp/-Leu/-His/-Ade and X-α-gal staining of the co-transformants confirmed the interaction between Pst18363 and TaNUDX23 in yeast (Fig. 4a).

In order to determine whether Pst18363 can directly interact with TaNUDX23, a GST pull-down assay was conducted. GST-fused TaNUDX23 proteins or GST protein was

This article is protected by copyright. All rights reserved

precipitated using glutathione beads and then incubated with His-fused Pst18363(ΔSP) protein. The immunoprecipitated protein complexes were detected by western blotting, which showed that the GST-fused TaNUDX23 proteins bound to His-Pst18363, whereas GST alone did not under the same conditions (Fig. 4b), indicating that Pst18363 interacts with TaNUDX23 *in vitro*.

To determine whether Pst18363 interacts with TaNUDX23 *in vivo*, BiFC was performed following *A. tumefaciens*-mediated transient expression in *N. benthamiana*. The plasmids nYFP-Pst18363/Pst18363-cYFP and nYFP-TaNUDX23/TaNUDX23-cYFP were co-infiltrated into *N. benthamiana* leaves by *A. tumefaciens*. The EVs (nYFP or cYFP) in combination with Pst18363-cYFP or nYFP-TaNUDX23 were used as negative controls. BiFC analysis showed that the strong YFP signal was observed in the combinations of Pst18363 and TaNUDX23, while no signal was detected in the negative control combination (Fig. 4c). In addition, we selected five homologs of TaNUDX23 based on phylogenetic analysis (Fig. S7a) to test their interaction relationships with Pst18363. BIFC assays showed that Pst18363 doesn't interact with the five homologs of TaNUDX23, suggesting Pst18363 interacts specifically with TaNUDX23 (Fig. S7b).

Subsequently, a CoIP experiment was conducted based on *A. tumefaciens*-mediated transient expression in *N. benthamiana*. Either YFP or Pst18363-YFP was co-expressed with TaNUDX23-mCherry into *N. benthamiana* leaves by *A. tumefaciens*. Total protein extracts were isolated from the *N. benthamiana* leaves infiltrated with *A. tumefaciens* at 48 hpi and subjected to a CoIP assay using GFP-Trap agarose beads (Chromotek). Western blot analysis showed that TaNUDX23-mCherry protein was immunoprecipitated and specifically detected with the anti-mCherry antibody in the presence of Pst18363-YFP, but not in the YFP control, whereas all constructs were detected in the relevant input fractions (Fig. 4d). Taken together, these results reveal that Pst18363 interacts with TaNUDX23 *in vivo*.

Pst18363 stabilizes TaNUDX23 proteins *in vivo*

This article is protected by copyright. All rights reserved

Accepted Article

To explore the effect of effector Pst18363 on TaNUDX23 *in vivo*, TaNUDX23-HA were transiently expressed together with Pst18363-Flag in *N. benthamiana*. Immuno-blot analysis showed that the protein level of TaNUDX23-HA was much higher when co-expressed with Pst18363-Flag than when co-expressed with the negative control GFP (Fig. 5a; Fig. S8). The result suggested that PST18363 potentially increases the stability of TaNUDX23. Because most protein degradation events are accomplished via the ubiquitin/26S proteasome pathway (Dreher & Callis, 2007), we tested whether TaNUDX23 was regulated by this pathway. As shown in Fig. 5a, the protein level of TaNUDX23 was increased by infiltrating proteasome inhibitor MG132, suggesting TaNUDX23 is degraded by the 26S proteasome pathway in plants. Moreover, we found that Pst18363 and MG132 didn't increase the transcript level of *TaNUDX23* by qRT-PCR analysis (Fig. 5b). Taken together, these results suggest that Pst18363 stabilizes TaNUDX23 by preventing its degradation mediated by the 26S proteasome.

TaNUDX23 is a functional nucleoside diphosphate hydrolase

As an interaction target of Pst18363, the function of TaNUDX23 remains unclear. First, we determined whether TaNUDX23 possesses nucleoside diphosphate hydrolase activity, using a general method for enzymatic activity of Nudix hydrolases (Ge *et al.*, 2007). GST protein and recombinant protein TaNUDX23-GST expressed in and purified from *E. coli* were analyzed by SDS-PAGE (Fig. 6a). In the enzymatic activity assay, substrates (nucleoside diphosphate-X) were hydrolyzed to generate phosphatase-sensitive products that, in the presence of intestinal phosphatase, released inorganic phosphate that was quantified colorimetrically. TaNUDX23 was found to be active on several known Nudix hydrolase substrates, such as ADPR, NADH, and FAD, but showed essentially no activity on UDP-Glc (Fig. 6b), indicating that TaNUDX23 is an active nucleoside diphosphate hydrolase. In later experiments, hydrolase activity of TaNUDX23 was completely inhibited in the presence of Ca^{2+} (Fig. 6c).

Because Pst18363 interacted with TaNUDX23, we proposed that Pst18363 can

This article is protected by copyright. All rights reserved

Accepted Article

directly either increase or decrease the hydrolase activity of TaNUDX23. To clarify this question, the Nudix hydrolase activity of mixtures containing purified GST and Pst18363-GST, purified GST and TaNUDX23-GST, or Pst18363-GST and TaNUDX23-GST were measured by comparing activity with purified GST. In these assays, substrates ADPR and NADH were used. As shown in Fig. S9, Nudix hydrolase activity of TaNUDX23-GST with Pst18363-GST was similar to that of TaNUDX23-GST without Pst18363-GST. These results indicate that Pst18363 does not directly affect the Nudix hydrolase activity of TaNUDX23.

TaNUDX23 decreases ROS accumulation

Several Nudix hydrolases can modulate redox balance in response to biotic or abiotic stress (Ge *et al.*, 2007; Ogawa *et al.*, 2009; Jambunathan *et al.*, 2010; Dong *et al.*, 2011). To explore whether TaNUDX23 plays a role in maintaining redox balance, the VIGS strategy was employed to knock down all three copies of the endogenous *TaNUDX23* genes (*TaNUDX23*-A/B/D) in the Su11 wheat. Two independent common fragments (TaNUDX23-1/2as) of *TaNUDX23*-A/B/D were designed for silencing the expression of *TaNUDX23* (Fig. S6a). The fourth leaves of wheat leaves inoculated with BSMV: γ or BSMV: TaNUDX23-1/2as displayed mild chlorotic mosaic symptoms, while leaves inoculated with BSMV: *TaPDSas*, as a positive control, showed photobleaching symptoms (Fig. S10), indicating that the BSMV-VIGS system functioned well. Thereafter, the silenced leaves were inoculated with the incompatible *Pst* isolate CYR23, which induced ROS production around the infected host tissues during infection. qRT-PCR analysis at 48 hpi indicated that endogenous *TaNUDX23* in wheat was silenced by the VIGS system (Fig. 7b). Meanwhile, we measured the ROS accumulation by staining the infected wheat tissues at 48 hpi with DAB. The ROS accumulation in the TaNUDX23-silenced lines was significantly higher than that in BSMV: γ-inoculated lines (Fig.7a, c). These results suggest that TaNUDX23 may suppress ROS accumulation.

In order to further confirm that TaNUDX23 suppresses ROS accumulation, we

This article is protected by copyright. All rights reserved

Accepted Article

introduced an YFP-tagged TaNUDX23 gene into wild type *Arabidopsis*. RT-PCR analysis showed that TaNUDX23 was transformed successfully into *Arabidopsis* generating Pro_{35S}:TaNUDX23-10-2/-5 plants (Fig. 7d). Consistent with the transcript level of TaNUDX23 in T3 generation of Pro_{35S}:TaNUDX23-10-2/-5 plants, the pyrophosphohydrolase activities toward ADP-ribose and NADH in the Pro35S:TaNUDX23-10-2/-5 plants were significantly higher than levels in the wild-type plants (Fig. S11). Next, flg22, inducing a rapid oxidative burst, were used for determining the capacity of TaNUDX23 to maintain redox balance in wild-type and transgenic plants. We found that the flg22-induced ROS accumulation in TaNUDX23 transgenic plants was markedly reduced compared with the wild type (Fig. 7e). In summary, these results indicate that TaNUDX23 has the ability to decrease ROS accumulation.

Because ROS is a crucial trigger of cell death and Pst18363 inhibits Pst322-triggered cell death, we also tested if the transient expression of TaNUDX23 suppresses Pst322-triggered cell death in *N. benthamiana*. *A. tumefaciens*-mediated transient expression in *N. benthamiana* was also used according to the above methods. As shown in Fig. 7f, no cell death symptoms were observed in regions of the leaf pre-infiltrated with *A. tumefaciens* carrying TaNUDX23-HA; Pst322-induced cell death symptoms were evident in regions pre-infiltrated with buffer or *A. tumefaciens* carrying eGFP; infiltration with *A. tumefaciens* carrying TaNUDX23-HA or eGFP alone did not elicit visible cell death. Thus, TaNUDX23, like its interaction target Pst18363, can suppress Pst322-triggered cell death. In addition, to further test if TaNUDX23 suppresses Pst322-triggered cell death by preventing ROS accumulation, DAB staining was used to examine the ROS levels in these infiltrated leaves. The DAB staining in the leaf regions infiltrated with TaNUDX23/Pst322 was much weaker compared with those infiltrated with Buffer/Pst322 and eGFP/Pst322 (Fig. 7g). These results indicated that TaNUDX23 can suppress Pst322-triggered cell death by preventing ROS accumulation.

Silencing of *TaNUDX23* attenuates *Pst* infection

This article is protected by copyright. All rights reserved

To examine the potential role of *TaNUDX23* in preventing or promoting stripe rust, we first analyzed the expression pattern of the *TaNUDX23* gene in response to the *Pst* infection. The results of qRT-PCR confirmed that the transcript levels of *TaNUDX23* were marginally elevated in Su11 wheat seedlings at 12, 24, 48 hpi with CYR31 (Fig. 8a). Furthermore, we used the VIGS approach to silence *TaNUDX23*. However, unlike the above, the silenced leaves were inoculated with the compatible *Pst* isolate CYR31. Remarkably, on wheat leaves inoculated with the TaNUDX23-1/2as silencing constructs and CYR31, sporulation was significantly reduced compared with the control plants inoculated with BSMV: γ and mock plants (Fig. 8b). qRT-PCR confirmed that expression of endogenous *TaNUDX23* was reduced in the BSMV:TaNUDX23-1/2as knockdown plants at 24 hpi and 48 hpi (Fig. 8c). Biomass analysis showed a significant reduction in both BSMV: TaNUDX23-1/2as silenced lines at 12 dpi with CYR31 (Fig. 8d). In addition, histological analysis by fluorescence microscope revealed that initial haustorium formation and growth of secondary hyphae are both reduced in BSMV: TaNUDX23-1/2as-silenced plants (Fig. 8e, f; Fig. S12). Interestingly, the hyphae in BSMV: TaNUDX23-1/2as-silenced plants at 48 hpi were strikingly swollen compared with those in BSMV: γ-inoculated plants, and the width of the swollen hyphae was much larger than that of the hyphae in BSMV: γ-inoculated plants (Fig. S12b, d). In summary, these results demonstrated that *Pst* infection in the *TaNUDX23*-silenced wheat was attenuated, suggesting that TaNUDX23 played an important role in promoting stripe rust.

Discussion

Obligate biotrophs including rust fungi, establish a close interaction with their living hosts for survival. Therefore, efficient strategies must be employed to thwart the host defense mechanisms and to suppress programmed cell death (PCD). To achieve this, rust fungi, like other pathogens, also secrete effectors into the host cell to promote colonization by regulating host immune responses. In this study, we screened an effector Pst18363

This article is protected by copyright. All rights reserved

Accepted Article

suppressing BAX-induced PCD, which is orthologous to *U. fabae* RTP1. RTP1 is the first rust secreted protein that is directly transferred from haustoria to host cells during infection (Kemen *et al.*, 2005). RTP homologues are most likely to be widespread in rust fungi and constitute a family of secreted effectors specific to rust fungi (Pretsch *et al.*, 2013), suggesting their importance to pathogenic processes in those pathogens. Using qRT-PCR and HIGS, we found that the *Pst* effector *Pst18363* is upregulated during the early infection stage (Fig. 1) and transient silencing of *Pst18363* attenuates pathogenicity of *Pst* (Fig. 2b), revealing it as a crucial virulence factor for *Pst* infection in wheat. Sequence analysis indicated that Pst18363, like Uf-RTP1, contains seven highly conserved β strands and two β-aggregation domains and four conserved cysteines at the C-terminus (Fig. S2b). Previous studies revealed that β-aggregation domains and four conserved cysteines of Uf-RTP1 are responsible for forming filamentous structures and cysteine protease inhibitor activity, respectively (Kemen *et al.*, 2013; Pretsch *et al.*, 2013). Further work needs to be performed to study whether Pst18363 has these abilities. Relative to other rust fungi RTP, Pst18363 has been shown to have a novel function that is to suppress cell death triggered by candidate effector Pst322 from *Pst* (Fig. 3), suggesting Pst18363 may regulate host immune responses to enable *Pst* growth during infection. Moreover, TaNUDX23 from wheat was identified as a major host target of Pst18363 by Y2H screening, and the interaction relationship between TaNUDX23 and Pst18363 was verified by Y2H, pull-down, BIFC and CoIP assays (Fig. 4).

Nudix hydrolases mainly catalyze organic pyrophosphates and can be divided into five subfamilies based on the substrate preference of these enzymes: ADP-sugar, Ap_nA, CoA, NAD(P)H and FAD pyrophosphohydrolases (Ogawa *et al.*, 2008). *A. thaliana* Nudix hydrolase AtNUDX23, the closest homolog of TaNUDX23, was reported to have pyrophosphohydrolase activity toward both FAD and ADP-ribose (Ogawa *et al.*, 2008). Our data showed that TaNUDX23 can hydrolyze ADP-ribose and FAD (Fig. 5b), which is consistent with pyrophosphohydrolase activity of AtNUDX23. Surprisingly, compared with AtNUDX23, TaNUDX23 possesses strong NADH pyrophosphohydrolase activity (Fig. 5b).

This article is protected by copyright. All rights reserved

Thus, TaNUDX23 is a Nudix hydrolase with multiple pyrophosphohydrolase activities.

Results of numerous studies indicate that the regulatory actions of Nudix hydrolases are closely related to immune responses to pathogens. And in many immune responses, ROS act as important signaling molecules. Our results showed that heterologous overexpression of *TaNUDX23* in *Arabidopsis* decreased the levels of ROS triggered by elicitor flg22 compared with the wild-type plants (Fig. 7e), coupled with the increasing ADP-ribose and NADH pyrophosphohydrolase activities in over-expression transgenic plants (Fig. S11). In addition, we found that ROS accumulation around the infection site in *TaNUDX23*-silenced plants at 48 hpi with the CYR23 was obviously higher than that in BSMV: γ-inoculated plants (Fig. 7a, c). These results indicate that TaNUDX23 can suppress the accumulation of ROS in plant cells, which is similar to a previous report that transient expression of Nudix hydrolase effector Avr3b reduces accumulation of ROS around *Phytophthora* infection sites (Dong *et al.*, 2011). NADH/NAD^+ turnover plays a key role in maintaining the ROS balance. AtNUDX7 and AtNUDX2 have been reported to maintain redox homeostasis in response to various stresses by nucleotide recycling from free ADP-ribose molecules (Ge *et al.*, 2007; Ishikawa *et al.*, 2009; Ogawa *et al.*, 2009; Jambunathan *et al.*, 2010). Thus, we propose, without sufficient verification, that TaNUDX23 suppresses the accumulation of ROS in plant cells by decreasing NADH levels and recycling nucleotides from free ADP-ribose with its hydrolase activity. Moreover, we found that transient expression of *TaNUDX23* in *N. benthamiana* can suppress PCD triggered by Pst322, along with a phenotype that ROS stained with DAB in the leaf regions infiltrated with TaNUDX23/Pst322 are much weaker compared with those infiltrated with eGFP/Pst322 (Fig. 7f, g). ROS at high concentration is a crucial inducer of cell death in plant (Petrov & Van Breusegem, 2012). Transient overexpression of plant catalases suppresses effector PsCRN63-triggered PCD by depressing ROS accumulation. Taking these results together with the result that silencing *TaNUDX23* in wheat attenuates *Pst* infection (Fig. 8b, d), we propose that TaNUDX23 negatively regulates immune responses, including PCD by depressing the accumulation of ROS.

This article is protected by copyright. All rights reserved

To increase virulence and pathogenicity, many pathogen effectors target and suppress host proteins associated with resistance (Deslandes & Rivas, 2012). Compared with the number of positive regulators of defense, relatively fewer negative regulators of host resistance have been reported to be directly targeted by effectors from pathogens. At present, negative regulators of host defense are targeted by pathogen effectors mainly to utilize them for infection. For instance, *P. sojae* effector PsAvh262 has been shown to suppress ER stress-triggered cell death and facilitate *Phytophthora* infection by binding to and stabilizing BIPs, which act as a negative regulators of plant resistance to *Phytophthora* (Jing *et al.*, 2016); and *P. infestans* effector Pi17316 has been shown to suppress immunity by targeting the MAP3K StVIK and utilizing or promoting its activity as a negative regulator of immunity (Murphy *et al.*, 2018). Presumably, Pst18363 may utilize the function of the negative regulator of defense TaNUDX23. This speculation is supported by the result that transient co-overexpression of *Pst18363* and *TaNUDX23* in *N. benthamiana* stabilizes TaNUDX23 (Fig. 5a).

In summary, our results revealed that an effector Pst18363 from *Pst* can target and stabilize a negative regulator of defense, which can suppress the accumulation of ROS during *Pst* infection. Future studies will focus on exploring whether Pst18363 inhibits plant cell death and regulates host immune responses that rely on the hydrolase activity of TaNUDX23.

Acknowledgements

This study was supported by National Natural Science Foundation of China (31430069 and 31620103913), National Key R&D Program of China (2018YFD0200402), and the 111 Project from the Ministry of Education of China (B07049).

Author Contributions

J. G. (Jun Guo) and Z. K. designed experiments. Q. Y., K. C., Y. L., B. H. and X. Z. performed the experiments. J. G. (Jia Guo) did the phylogenetic analysis. Q. Y., J. G. (Jun

This article is protected by copyright. All rights reserved

Accepted Article

Guo) and Z. K. wrote the manuscript.

References

Bartsch M, Gobbato E, Bednarek P, Debey S, Schultze J, Bautor J, Parker J. 2006. Salicylic acid-independent ENHANCED DISEASE SUSCEPTIBILITY1 signaling in *Arabidopsis* immunity and cell death is regulated by the monooxygenase *FMO1* and the nudix hydrolase *NUDT7*. *Plant Cell* **18**(4): 1038-1051.

Bessman M, Frick D, OHandley S. 1996. The MutT proteins or "nudix" hydrolases, a family of versatile, widely distributed, "housecleaning" enzymes. *Journal of Biological Chemistry* **271**(41): 25059-25062.

Bos J, Kanneganti T, Young C, Cakir C, Huitema E, Win J, Armstrong M, Birch P, Kamoun S. 2006. The C-terminal half of *Phytophthora infestans* RXLR effector AVR3a is sufficient to trigger R3a-mediated hypersensitivity and suppress INF1-induced cell death in *Nicotiana benthamiana*. *The Plant Journal* **48**(2): 165-176.

Chen X. 2014. Integration of cultivar resistance and fungicide application for control of wheat stripe rust. *Canadian Journal Of Plant Pathology* **36**(3): 311-326.

Chisholm S, Coaker G, Day B, Staskawicz B. 2006. Host-Microbe interactions: Shaping the evolution of the plant immune response. *Cell* **124**(4): 803-814.

Deslandes L, Rivas S. 2012. Catch me if you can: Bacterial effectors and plant targets. *Trends in Plant Science* **17**(11): 644-655.

Dong S, Yin W, Kong G, Yang X, Qutob D, Chen Q, Kale S, Sui Y, Zhang Z, Dou D *et al*. 2011. *Phytophthora sojae* avirulence effector Avr3b is a secreted NADH and ADP-ribose pyrophosphorylase that modulates plant immunity. *PLoS Pathogens* **7**(11): e1002353.

Dou D, Kale S, Wang X, Chen Y, Wang Q, Wang X, Jiang R, Arredondo F, Anderson R, Thakur P *et al*. 2008. Conserved C-terminal motifs required for avirulence and

This article is protected by copyright. All rights reserved

Accepted Article

suppression of cell death by *Phytophthora sojae* effector Avr1b. *Plant Cell* **20**(4): 1118-1133.

Dreher K, Callis J. 2007. Ubiquitin, hormones and biotic stress in plants. *Annals of Botany* **99**(5): 787-822.

Dunn C, O'Handley S, Frick D, Bessman M. 1999. Studies on the ADP-ribose pyrophosphatase subfamily of the Nudix hydrolases and tentative identification of *trgB*, a gene associated with tellurite resistance. *Journal of Biological Chemistry* **274**(45): 32318-32324.

Fan G, Yang Y, Li T, Lu W, Du Y, Qiang X, Wen Q, Shan W. 2018. A *Phytophthora capsici* RXLR effector targets and inhibits a plant PPIase to suppress endoplasmic reticulum-mediated immunity. *Molecular Plant* **11**(8): 1067-1083.

Ge X, Li G, Wang SB, Zhu H, Zhu T, Wang X, Xia Y. 2007. *AtNUDT7*, a negative regulator of basal immunity in *Arabidopsi*s, modulates two distinct defense response pathways and is involved in maintaining redox homeostasis. *Plant Physiology* **145**(1): 204-215.

Gunawardana D, Likic V, Gayler K. 2009. A comprehensive bioinformatics analysis of the nudix superfamily in *Arabidopsis thaliana*. *Comparative and Functional Genomics* **2009**: 1-13.

Holzberg S, Brosio P, Gross C, Pogue G. 2002. Barley stripe mosaic virus-induced gene silencing in a monocot plant. *The Plant Journal* **30**(3): 315-327.

Ishikawa K, Ogawa T, Hirosue E, Nakayama Y, Harada K, Fukusaki E, Yoshimura K, Shigeoka S. 2009. Modulation of the Poly(ADP-ribosyl)ation reaction via the *Arabidopsis* ADP-Ribose/NADH pyrophosphohydrolase, *AtNUDX7*, is involved in the response to oxidative stress. *Plant Physiology* **151**(2): 741–754.

Jacobs K, Collins-Racie L, Colbert M, Duckett M, Golden-Fleet M, Kelleher K, Kriz R, LaVallie E, Merberg D, Spaulding V *et al*. 1997. A genetic selection for isolating cDNAs encoding secreted proteins. *Gene* **198**(1): 289-296.

Jambunathan N, Mahalingam R. 2006. Analysis of *Arabidopsis Growth Factor Gene 1*

This article is protected by copyright. All rights reserved

Accepted Article

(*GFG1*) encoding a nudix hydrolase during oxidative signaling. *Planta* **224**(1): 1-11.

Jambunathan N, Penaganti A, Tang Y, Mahalingam R. 2010. Modulation of redox homeostasis under suboptimal conditions by *Arabidopsis* nudix hydrolase 7. *BMC Plant Biology* **10**(1): 173.

Jamir Y, Guo M, Oh H, Petnicki-Ocwieja T, Chen S, Tang X, Dickman M, Collmer A, R. Alfano J. 2004. Identification of *Pseudomonas syringae* type III effectors that can suppress programmed cell death in plants and yeast. *The Plant Journal* **37**(4): 554-565.

Jing M, Guo B, Li H, Yang B, Wang H, Kong G, Zhao Y, Xu H, Wang Y, Ye W *et al*. 2016. A *Phytophthora sojae* effector suppresses endoplasmic reticulum stress-mediated immunity by stabilizing plant Binding immunoglobulin Proteins. *Nature Communications* **7**: 11685.

Jones J, Dangl J. 2006. The plant immune system. *Nature* **444**(7117): 323-329.

Kang Z, Huang LL, Buchenauer H. 2002. Ultrastructural changes and localization of lignin and callose in compatible and incompatible interactions between wheat and *Puccinia striiformis*. *Journal of Plant Diseases and Protection* **109**(1): 25-37.

Kemen E, Kemen A, Ehlers A, Voegele R, Mendgen K. 2013. A novel structural effector from rust fungi is capable of fibril formation. *The Plant Journal* **75**(5): 767-780.

Kemen E, Kemen A, Rafiqi M, Hempel U, Mendgen K, Hahn M, Voegele R. 2005. Identification of a protein from rust fungi transferred from haustoria into infected plant cells. *Molecular Plant–Microbe Interactions* **18**(11): 1130-1139.

Kraszewska E. 2008. The plant Nudix hydrolase family. *Acta Biochimica Polonica* **55**(4): 663-671.

Line R. 2002. Stripe rust of wheat and barley in North America: A retrospective historical review. *Annual Review of Phytopathology* **40**(1): 75-118.

Liu C, Pedersen C, Schultz-Larsen T, Aguilar G, Madriz-Ordenana K, Hovmoller M, Thordal-Christensen H. 2017. The stripe rust fungal effector PEC6 suppresses pattern-triggered immunity in a host species-independent manner and interacts with

This article is protected by copyright. All rights reserved

Accepted Article

adenosine kinases. *New Phytologist* **213**(3): 1556-1556.

Liu J, Guan T, Zheng P, Chen L, Yang Y, Huai B, Li D, Chang Q, Huang L, Kang Z. 2016. An extracellular Zn-only superoxide dismutase from *Puccinia striiformis* confers enhanced resistance to host-derived oxidative stress. *Environmental Microbiology* **18**(11): 4118-4135.

Livak K, Schmittgen T. 2001. Analysis of relative gene expression data using Real-Time quantitative PCR and the $2^{-\Delta\Delta CT}$ method. *Methods* **25**(4): 402-408.

McLennan A. 2006. The Nudix hydrolase superfamily. *Cellular and Molecular Life Sciences* **63**(2): 123-143.

Murphy F, He Q, Armstrong M, Giuliani L, Boevink P, Zhang W, Tian Z, Birch P, Gilroy E. 2018. Potato *MAP3K StVIK* is required for *Phytophthora infestans* RXLR effector Pi17316 to promote disease. *Plant Physiology* **177**(1): 398-410.

Ogawa T, Ishikawa K, Harada K, Fukusaki E, Yoshimura K, Shigeoka S. 2009. Overexpression of an ADP-ribose pyrophosphatase, *AtNUDX2*, confers enhanced tolerance to oxidative stress in *Arabidopsis* plants. *The Plant Journal* **57**(2): 289-301.

Ogawa T, Yoshimura K, Miyake H, Ishikawa K, Ito D, Tanabe N, Shigeoka S. 2008. Molecular characterization of Organelle-Type nudix hydrolases in *Arabidopsis*. *Plant Physiology* **148**(3): 1412-1424.

Oh S, Young C, Lee M, Oliva R, Bozkurt T, Cano L, Win J, Bos J, Liu H, van Damme M *et al*. 2009. In planta expression screens of *Phytophthora infestans* RXLR effectors reveal diverse phenotypes, including activation of the solanum bulbocastanum disease resistance protein *Rpi-blb2*. *Plant Cell* **21**(9): 2928-2947.

Petrov V, Van Breusegem F. 2012. Hydrogen peroxide—a central hub for information flow in plant cells. *AoB Plants* **2012**: pls014.

Pretsch K, Kemen A, Kemen E, Geiger M, Mendgen K, Voegele R. 2013. The rust transferred proteins-a new family of effector proteins exhibiting protease inhibitor function. *Molecular Plant Pathology* **14**(1): 96-107.

Shan W, Cao M, Leung D, Tyler B. 2004. The *Avr1b* locus of *Phytophthora sojae*

This article is protected by copyright. All rights reserved

Accepted Article

encodes an elicitor and a regulator required for avirulence on soybean plants carrying resistance gene *Rps1b*. *Molecular Plant–Microbe Interactions* **17**(4): 394-403.

Tamura N, Murata Y, Mukaihara T. 2005. Isolation of *Ralstonia solanacearum hrpB* constitutive mutants and secretion analysis of *hrpB*-regulated gene products that share homology with known type III effectors and enzymes. *Microbiology* **151**(9): 2873-2884.

Voinnet O, Rivas S, Mestre P, Baulcombe D. 2003. An enhanced transient expression system in plants based on suppression of gene silencing by the p19 protein of tomato bushy stunt virus. *The Plant Journal* **33**(5): 949-956.

Wang X, Wang X, Feng H, Tang C, Bai P, Wei G, Huang L, Kang Z. 2012. *TaMCA4*, a novel wheat metacaspase gene functions in programmed cell death induced by the fungal pathogen *Puccinia striiformis* f. sp. *tritici*. *Molecular Plant-Microbe Interactions* **25**(6): 755-764.

Wang X, Yang B, Li K, Kang Z, Cantu D, Dubcovsky J. 2016. A conserved *Puccinia striiformis* protein interacts with wheat NPR1 and reduces induction of pathogenesis-related genes in response to pathogens. *Molecular Plant–Microbe Interactions* **29**(12): 977-989.

Wang Y, Li J, Hou S, Wang X, Li Y, Ren D, Chen S, Tang X, Zhou J. 2010. A *Pseudomonas syringae* ADP-ribosyltransferase inhibits *Arabidopsis* mitogen-activated protein kinase kinases. *Plant Cell* **22**(6): 2033-2044.

Wellings C. 2011. Global status of stripe rust: A review of historical and current threats. *Euphytica* **179**(1SI): 129-141.

Win J, Kamoun S, Jones A. 2011. Purification of effector-target protein complexes via transient expression in *Nicotiana benthamiana*. *Methods in Molecular Biology*, **712**: 181-194.

Xiao S, Ellwood S, Calis O, Patrick E, Li T, Coleman M, Turner J. 2001. Broad-spectrum mildew resistance in *Arabidopsis thaliana* mediated by *RPW8*. *Science* **291**(5501): 118-120.

This article is protected by copyright. All rights reserved

Accepted Article

Yin W, Wang Y, Chen T, Lin Y, Luo C. 2018. Functional evaluation of the signal peptides of secreted proteins. *Bio-Protocol* **8**(9).

Zhang J, Shao F, Cui H, Chen L, Li H, Zou Y, Long C, Lan L, Chai J, Chen S *et al*. 2007. A *Pseudomonas syringae* effector inactivates *MAPKs* to suppress PAMP-Induced immunity in plants. *Cell Host & Microbe* **1**(3): 175-185.

Zhang M, Li Q, Liu T, Liu L, Shen D, Zhu Y, Liu P, Zhou J, Dou D. 2014. Two cytoplasmic effectors of *Phytophthora sojae* regulate plant cell death via interactions with plant catalases. *Plant Physiology* **167**(1): 164-175.

Zheng W, Huang L, Huang J, Wang X, Chen X, Zhao J, Guo J, Zhuang H, Qiu C, Liu J *et al*. 2013. High genome heterozygosity and endemic genetic recombination in the wheat stripe rust fungus. *Nature Communications* **4:**2673.

Accepted Article

This article is protected by copyright. All rights reserved

Supporting information

Fig. S1 Effector Pst18363 in *Pst* suppresses plant cell death triggered by BAX in *N. benthamiana.*

Fig. S2 Phylogenetic analysis and multiple sequence alignment of Pst18363 and its homologs.

Fig. S3 Functional validation of the signal peptide of Pst18363.

Fig. S4 Histological observation of fungal growth in *Pst18363*-knockdown plants**.**

Fig. S5 BIFC assays for screening the interaction between Pst18363 and candidate targets.

Fig. S6 Alignment of the TaNUDX23-A, TaNUDX23-B and TaNUDX23-D coding regions and proteins.

Fig. S7 Phylogenetic analysis of NUDX proteins and BIFC assays for the interaction between Pst18363 and TaNUDX proteins.

Fig. S8 Original western-blots shown in Figure 5.

Fig. S9 Pst18363 does not influence Nudix hydrolase activity of TaNUDX23.

Fig. S10 Symptoms on the fourth leaves of the wheat plants inoculated with BSMV: γ or BSMV: TaNUDX23-1/2as.

Fig. S11 Overexpression of *TaNUDX23* in *Arabidopsis* increases ADP-ribose and NADH activities.

Fig. S12 Histological observation of fungal growth in *TaNUDX23*-knockdown plants.

Table S1 Primers used in this study.

Table S2 Reciprocal BLASTP searches on the *Pst* and *Uromyces fabae* genome databases.

Table S3 The full-length coding sequences of *Pst24948* and *Pst09949*.

Table S4 The list of Pst18363IPs identified by Y2H.

This article is protected by copyright. All rights reserved

Accepted Article

Figure legends

Fig. 1 Relative transcript levels of *Pst18363* at different *Pst* infection stages. Wheat leaves (Su11) inoculated with fresh urediospores (CYR32) were sampled at different time points according to the infection stage of *Pst*. US (Urediospores) was used as a control. Relative transcript levels of *Pst18363* were calculated by the comparative threshold ($2^{-\Delta\Delta CT}$) method. The quantitative RT-PCR values were normalized to the transcript level of *PstEF-1.* The transcript level of *Pst18363* during *Pst* infection stages at the urediospores stage was standardized to 1. Values represent the means ± standard errors of three independent biological samples. Differences between time-course points were assessed using Student's t-tests. Asterisks indicate $P < 0.05$, double asterisks indicate $P < 0.01$. hpi, hours post inoculation.

Fig. 2 BSMV-mediated host-induced gene silencing (HIGS) of *Pst18363* reduced virulence of *Pst.* (a) Wheat leaves infected with BSMV: TaPDS, which showed photobleaching phenotype, was used as control. Mild chlorotic mosaic symptoms were observed on the fourth leaves of the wheat inoculated with BSMV: γ, BSMV: Pst18363-1/2as, BSMV: Pst24948-1/2as and BSMV: Pst09949-1/2as. (b) Phenotypes of the fourth leaves of knockdown plants or control plants inoculated with *Pst* race CYR32 at 12 dpi. The wheat leaves inoculated with BSMV: γ and BSMV: Pst24948-1/2as were used as negative controls. The wheat leaves inoculated with BSMV: *Pst09949*-1/2as were used as positive control. (c) Relative transcript levels of *Pst18363, Pst24948* and *Pst09949* were measured in knockdown plants at 120 hpi. Data were normalized to the transcript level of *PstEF-1*. (d) Relative *Pst* biomass ratio was measured via total DNA content of the knockdown-wheat leaves at 12 dpi inoculated with CYR32. Values represent the means ± standard errors of three independent biological samples. Differences were assessed using Student's t-tests. Asterisks indicate $P < 0.05$ and double asterisks indicate $P < 0.01$.

This article is protected by copyright. All rights reserved

Fig. 3 Suppression of Pst322-triggered cell death by Pst18363. (a) Pst18363 suppressed Pst322-triggered cell death. $MgCl_2$ buffer or *A. tumefaciens* cells carrying the Pst18363-HA or eGFP vector were infiltrated into the leaf of *N. benthamiana* within the regions indicated by the dashed lines, followed after 24 h by either no further infiltration (left side) or infiltration with *A. tumefaciens* cells carrying the Pst322 (right side). The phenotype of cell death was scored and photographed at 5 days after infiltration with Pst322. The bottom panel shows the same leaf as the top panel after decolorization with ethanol. (b) The mean percentages of sites showing cell death in leaves with different treatments was measured to assess the ability of Pst18363 to suppress Pst322-induced cell death. Differences between different treatments plants and control were assessed using Student's t-tests. The standard errors were scored from 15 infiltration sites based on three independent experiments using *N. benthamiana* leaves expressing Pst18363. Asterisks indicate $P < 0.05$ and double asterisks indicate $P < 0.01$. (c) RT-PCR was performed to confirm the expression of *Pst18363* and *Pst322* in each infiltration site with specific primers for *Pst18363* and *Pst322*. *NbEF1α* was used as a reference gene. (d) Western blot was performed to show normal expression of eGFP, Pst18363-HA and Pst322 in tobacco leaves using anti-GFP antibody, anti-HA antibody and anti-Flag antibody. (e) Wheat leaves (Su11) were transformed by bombardment with plasmid mixtures including EV+EV+GUS, EV+GUS+Pst322, and GUS+Pst322+Pst18363, respectively. The leaves were incubated for 48 hours in darkness at 28 °C after bombardment, and then stained with X-gluc. GUS, β-glucuronidase expression vector; EV, empty vector. (f) Number of GUS-positive blue spots following bombardment with plasmid mixtures, including EV+EV+GUS, EV+GUS+Pst322, and GUS+Pst322+Pst18363. The leaves bombarded with EV+EV+GUS were used as controls. Values represent mean ± standard errors from three independent replicates. Differences between control and wheat leaves with different treatments were assessed using Student's t-tests. Asterisks indicate $P < 0.05$ and double asterisks indicate $P < 0.01$.

This article is protected by copyright. All rights reserved

Fig. 4 Pst18363 interacts with TaNUDX23 *in vitro* and *in vivo*. (a) Pst18363 interacts with TaNUDX23 in yeast. Yeast strain AH109 co-carrying pGBKT7 (BD) or bait vector BD-Pst18363 and pGADT7 (AD) or prey vector AD-TaNUDX23 were grown on SD/-Trp/-Leu and the selective medium SD/-Trp/-Leu/-His/-Ade. Only the yeast co-expressing Pst18363 and TaNUDX23 grew on the medium SD/-Trp/-Leu/-His/-Ade and yielded X-α-gal activity. BD+AD, BD+ AD-TaNUDX23 and AD+BD-Pst18363 were used as negative controls. SD, synthetic dropout growth medium. (b) Pst18363 interacts with TaNUDX23 *in vitro*. Protein TaNUDX23-GST or GST purified by glutathione agarose were incubated with an equal amount of *E. coli* lysates containing His-Pst18363 for 1 h at 4 °C before glutathione eluent was added. Pulled-down proteins were detected by western blots using anti-GST antibody or anti-His antibody. The red asterisks represent protein TaNUDX23-GST. (c) Pst18363 interacts with TaNUDX23 *in planta*. The leaves of *N. benthamiana* were infiltrated with *Agrobacterium* strains containing the following construct pairs, Pst18363-cYFP+nYFP, nYFP-TaNUDX23+cYFP, nYFP-TaNUDX23+ Pst18363-cYFP, or TaNUDX23-cYFP+nYFP-Pst18363. The infiltrated *N. benthamiana* leaves were observed via fluorescence microscopy. Bars, 50 μm. (d) Pst18363 interacts with TaNUDX23 in plant cells. Protein was extracted from *N. benthamiana* tissues co-infiltrated with the indicated plasmid combinations (YFP+TaNUDX23-mCherry, Pst18363-YFP+TaNUDX23-mCherry) and immunoprecipitated with GFP-Trap. Immunoblot analysis was performed using anti-mCherry and anti-GFP antibodies. The red asterisks represent objective proteins YFP and Pst18363-YFP.

Fig. 5 Pst18363 stabilizes TaNUDX23 in *N. benthamiana*. (a) Analysis of the protein stability of TaNUDX23 by western blotting. Total protein was extracted from samples collected and immunoblotted using anti-HA, anti-Flag, and anti-GFP antibodies to detect TaNUDX23, Pst18363(ΔSP) and GFP, respectively. *A. tumefaciens* cells carrying the TaNUDX23-HA construct were co-infiltrated into *N. benthamiana* leaves with cells carrying GFP or Pst18363(ΔSP)-Flag. In the experiments, leaves were treated with 100

This article is protected by copyright. All rights reserved

Accepted Article

mM MG132 24 h after infiltration with *A. tumefaciens* cells. The infiltrated leaves were harvested 24 h after treatment with MG132. Ponceau S represents staining of the membrane to show equal loading. (b) Transcript levels of *TaNUDX23* determined by qRT-PCR. Relative transcript levels of *TaNUDX23* were calculated by the comparative threshold ($2^{-\Delta\Delta CT}$) method. The qRT-PCR values were normalized to the transcript level for *NbEF*, and the GFP+TaNUDX23 control was set to 1. Values represent the means ± standard errors of three independent samples.

Fig. 6 TaNUDX23 is a nucleoside diphosphate hydrolase. (a) SDS-PAGE analysis of recombinant protein GST-TaNUDX23 purified from *E. coli*. The first four lanes are soluble protein extracts of the *E. coli* carrying GST or GST-TaNUDX23 with or without induction of the recombinant protein by IPTG. The fifth lane shows purified recombinant protein GST-TaNUDX23. The protein bands were visualized by Coomassie staining. The blue and red asterisks represented objective proteins GST and GST-TaNUDX23, respectively. (b) Hydrolase activities of TaNUDX23 against several nucleotides. The intensity of the blue color is directly related to the TaNUDX23 activity. The reaction was carried out for each substrate in the presence of the purified TaNUDX23 protein or GST protein. Protein GST was used as a negative control. Nudix hydrolase substrates include Adenosine 5′-diphosphoribose (ADP-ribose; ADPR), reduced nicotinamide adenine dinucleotide (NADH), uridine 5′-diphosphoglucose (UDP-Glc), flavine adenine dinucleotide (FAD). (c) The activity of TaNUDX23 is completely inhibited by Ca^{2+}. The mixture reactions (left) were carried out for substrate NADH in the absence (-) of the purified protein or in the presence of the purified GST or TaNUDX23 protein. Each reaction (right) was supplemented with 7 mM Ca^{2+}.

Fig. 7 TaNUDX23 decreases ROS accumulation and suppresses Pst322-triggered cell death. (a) Histological observation after DAB staining of wheat leaves pre-treated with BSMV: γ or BSMV: TaNUDX23-1/2as and infected with CYR23 at 48 hpi. Bar, 50 μm. (b)

This article is protected by copyright. All rights reserved

Relative transcript level of *TaNUDX23* was decreased in *TaNUDX23*-knockdown plants inoculated with CYR23 at 48 hpi. The quantitative RT-PCR values were normalized to those for TaEF-1α. The transcript level of *TaNUDX23* in BSMV: γ plants was standardized as 1 at 48 hpi. Values represent the means ± standard errors of three independent samples. Differences were assessed using Student's t-tests. Double asterisks indicate $P < 0.01$. (c) The accumulation of H_2O_2 was measured by calculating the 3,3-diaminobenzidine (DAB)-stained area at each infection site using the DP-BSW software (Olympus Corp.) at 48 hpi. All results were obtained from 50 infection sites. Values represent the means ± standard errors of three independent samples. Differences were assessed using Student's t-tests. Asterisks indicate $P < 0.05$ and double asterisks indicate $P < 0.01$. (d) RT-PCR was performed to confirm the expression of *TaNUDX23* in *TaNUDX23* over-expression *Arabidopsis thaliana*. Wild-type plant (WT) was used as a negative control. *Atactin2* was used as a reference gene. (e) Reactive oxygen species (ROS) burst induced by 100 nM flg22 in discs of *A. thaliana* transgenic *TaNUDX23* and WT leaves. The results are representative of three independent experiments. Each data point consists of six replicates. Error bars indicate standard deviation. Student's t-test was carried out to determine the significance of the difference between the TaNUDX23 transgenic plants and WT in the same treatment. (f) TaNUDX23 suppressed Pst322-triggered cell death. $MgCl_2$ buffer or *A. tumefaciens* cells carrying the TaNUDX23-HA or eGFP vector were infiltrated into the leaf of *N. benthamiana* within the regions indicated by the dashed lines, followed after 24 h by either no further infiltration (left side) or by infiltration with *A. tumefaciens* cells carrying the Pst322 (right side). eGFP was used as a negative control. The phenotype of cell death was photographed at 5 days after infiltration with Pst322. (g) H_2O_2 production in *N. benthamiana* leaves was determined by DAB staining. *N. benthamiana* leaves were infiltrated with *A. tumefaciens* cells carrying the TaNUDX23-HA or eGFP vector, followed after 24 h by infiltration with *A. tumefaciens* cells carrying the Pst322. The measurement was performed 3 d after infiltration with Pst322.

This article is protected by copyright. All rights reserved

Fig. 8 *TaNUDX23* is a negative regulator of wheat immunity to *Pst*. (a) Transcript levels of *TaNUDX23* at different stages during *Pst* CYR31 infection were determined by qRT-PCR. Total RNA was extracted from wheat leaves infected with CYR31 at 0, 12, 24, 48, 72 and 120 h post inoculation (hpi). Relative transcript levels of *TaNUDX23* were calculated by the comparative threshold ($2^{-\Delta\Delta CT}$) method. The qRT-PCR values were normalized to the transcript level for *TaEF-1α* and are presented as fold changes relative that in untreated plants at time 0. (b) Phenotypes of the fourth leaves of knockdown plants inoculated with *Pst* race CYR31 at 12 dpi. (c) Transcript levels of *TaNUDX23* in *TaNUDX23*-knockdown plants at 24 and 48 hpi. (d) *Pst* and wheat biomass ratio at 12 dpi was measured via total DNA content of the knockdown-wheat leaves inoculated with CYR31. (e) The fungal structures were stained with wheat germ agglutinin (WGA) in wheat leaves inoculated with BSMV: γ or BSMV: TaNUDX23-1/2as and *Pst* at 120 hpi, and were observed under a fluorescence microscope. SV, sub-stomatal vesicle; IH, infection hypha. (f) Infection area of elongating hyphae in BSMV-infected plants inoculated with the CYR31 isolate at 120 hpi was calculated by DP-BSW software. All results were obtained from 50 infection sites. Values represent the means ± standard errors of three independent samples. Differences were assessed using Student's t-tests. Asterisks indicate $P < 0.05$ and double asterisks indicate $P < 0.01$.

Accepted Article

This article is protected by copyright. All rights reserved

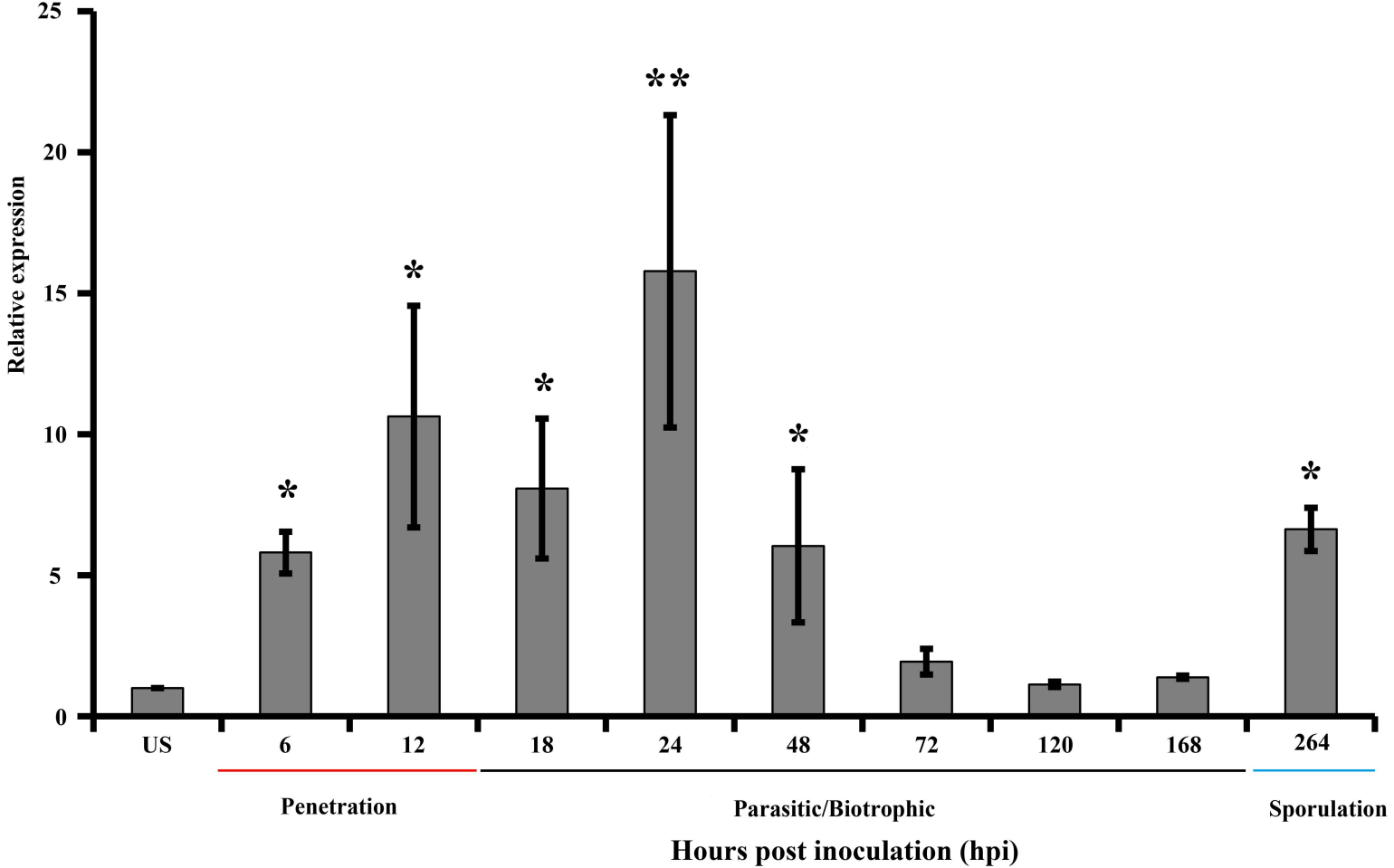
25
20
15
10
5
0
Relative expression
*
*
*
**
*
*
US
6
12
18
24
48
72
120
168
264
Penetration
Parasitic/Biotrophic
Sporulation
Hours post inoculation (hpi)

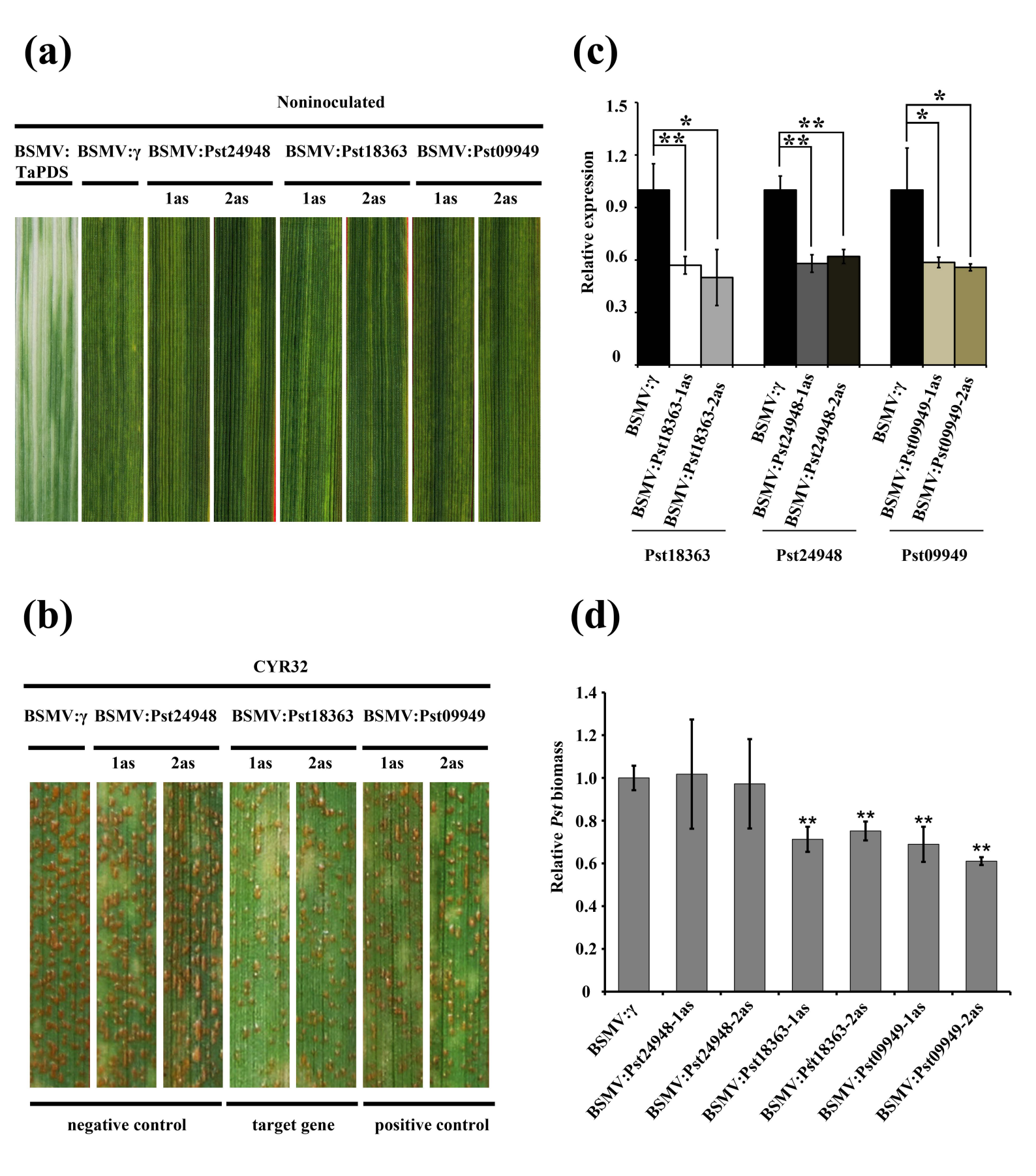
(a)
Noninoculated
BSMV: TaPDS
BSMV:γ
BSMV:Pst24948
BSMV:Pst18363
BSMV:Pst09949
1as
2as
1as
2as
1as
2as
(b)
CYR32
BSMV:γ
BSMV:Pst24948
BSMV:Pst18363
BSMV:Pst09949
1as
2as
1as
2as
1as
2as
negative control
target gene
positive control
(c)
Relative expression
1.5
1.2
0.9
0.6
0.3
0
*
**
**
**
*
*
BSMV:γ
BSMV:Pst18363-1as
BSMV:Pst18363-2as
BSMV:γ
BSMV:Pst24948-1as
BSMV:Pst24948-2as
BSMV:γ
BSMV:Pst09949-1as
BSMV:Pst09949-2as
Pst18363
Pst24948
Pst09949
(d)
Relative Pst biomass
1.4
1.2
1.0
0.8
0.6
0.4
0.2
0
**
**
**
**
BSMV:γ
BSMV:Pst24948-1as
BSMV:Pst24948-2as
BSMV:Pst18363-1as
BSMV:Pst18363-2as
BSMV:Pst09949-1as
BSMV:Pst09949-2as

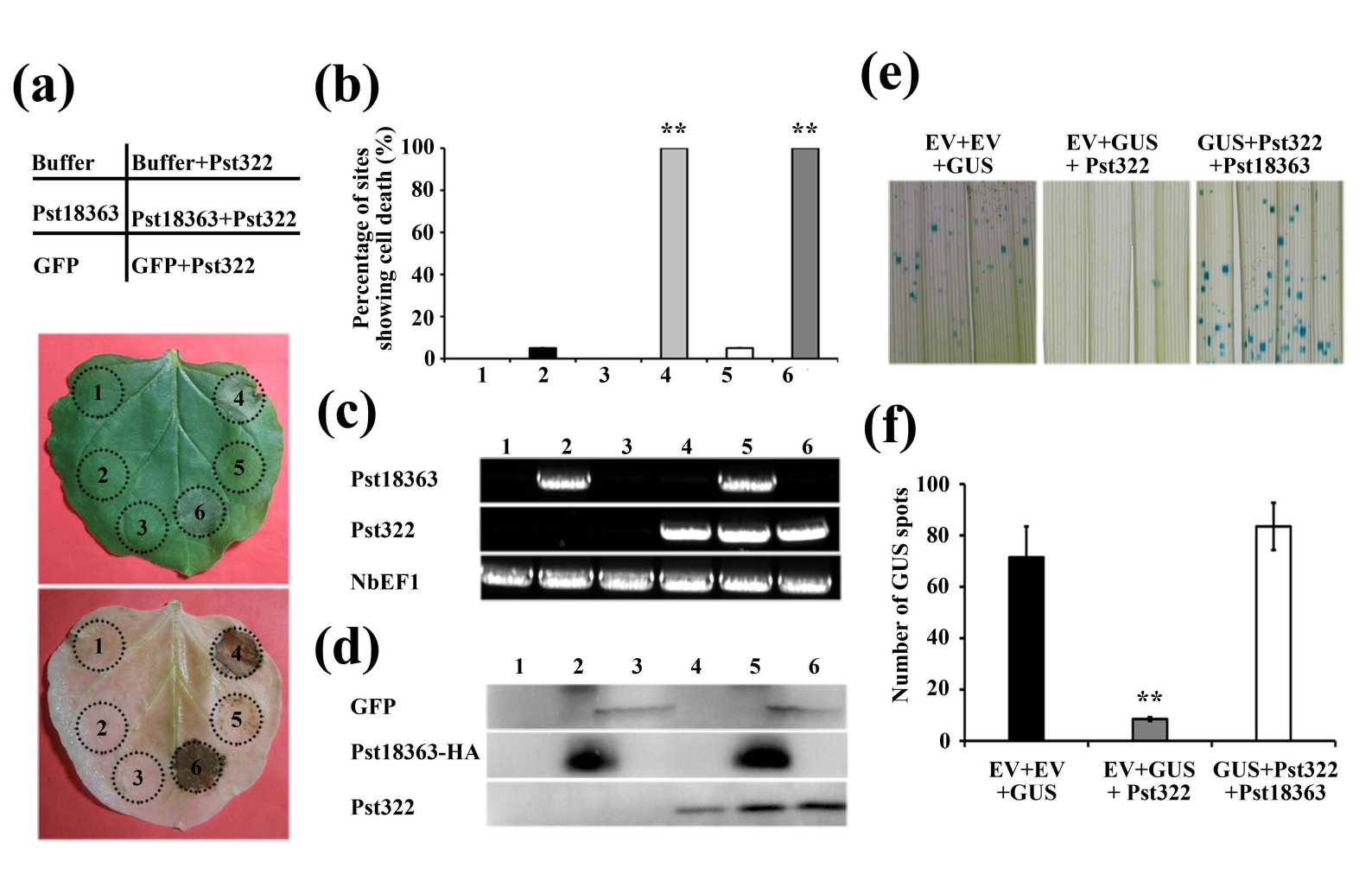
(a)
Buffer
Buffer+Pst322
Pst18363
Pst18363+Pst322
GFP
GFP+Pst322
1
2
3
4
5
6
(b)
Percentage of sites showing cell death (%)
100
80
60
40
20
0
**
**
1
2
3
4
5
6
(c)
1 2 3 4 5 6
Pst18363
Pst322
NbEF1
(d)
1 2 3 4 5 6
GFP
Pst18363-HA
Pst322
(e)
EV+EV +GUS
EV+GUS + Pst322
GUS+Pst322 +Pst18363
(f)
Number of GUS spots
100
80
60
40
20
0
**
EV+EV +GUS
EV+GUS + Pst322
GUS+Pst322 +Pst18363

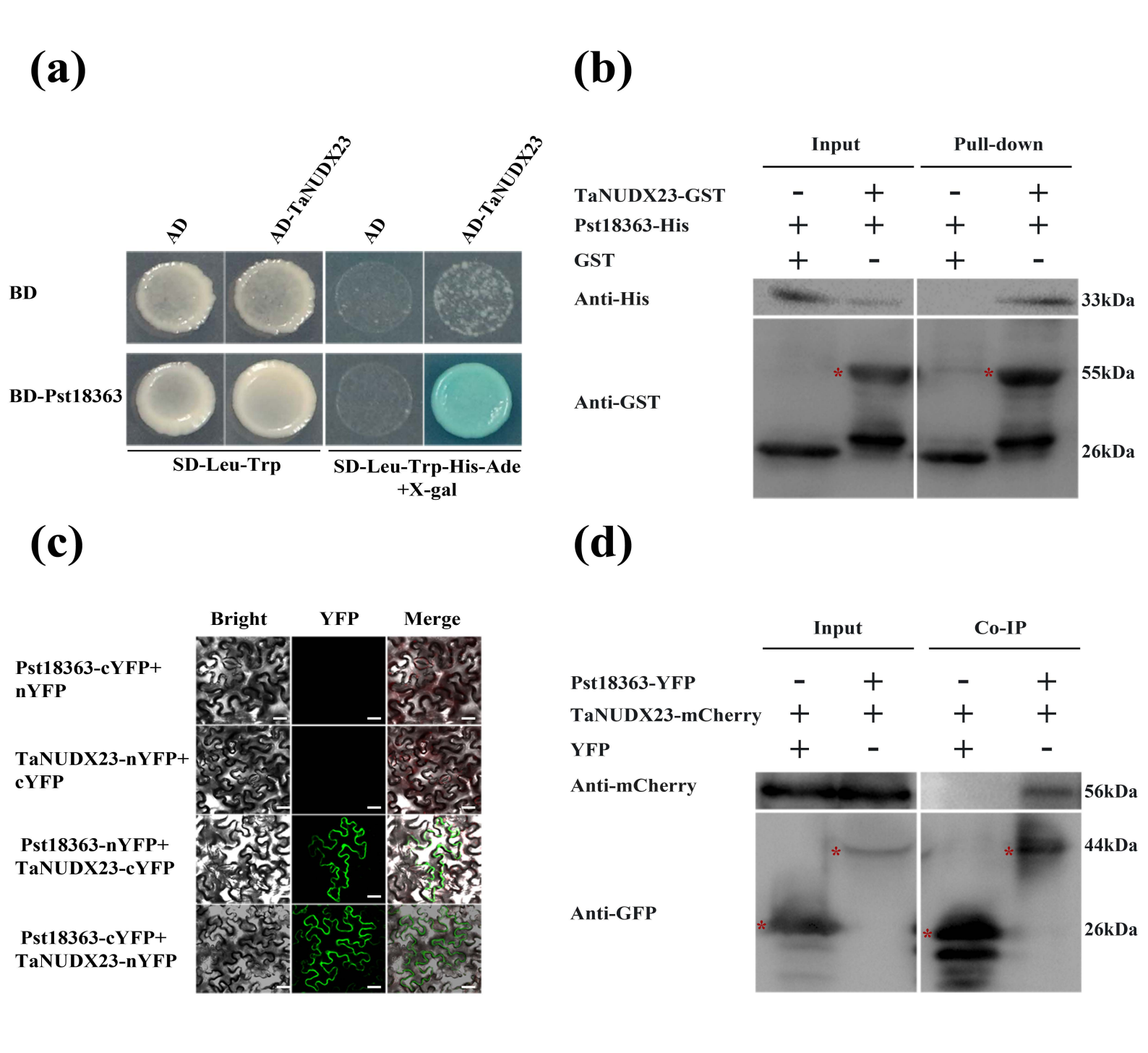
(a)
AD
AD-TaNUDX23
AD
AD-TaNUDX23
BD
BD-Pst18363
SD-Leu-Trp
SD-Leu-Trp-His-Ade
+X-gal
(b)
Input
Pull-down
TaNUDX23-GST
Pst18363-His
GST
Anti-His
Anti-GST
33kDa
55kDa
26kDa
(c)
Bright
YFP
Merge
Pst18363-cYFP+
nYFP
TaNUDX23-nYFP+
cYFP
Pst18363-nYFP+
TaNUDX23-cYFP
Pst18363-cYFP+
TaNUDX23-nYFP
(d)
Input
Co-IP
Pst18363-YFP
TaNUDX23-mCherry
YFP
Anti-mCherry
Anti-GFP
56kDa
44kDa
26kDa

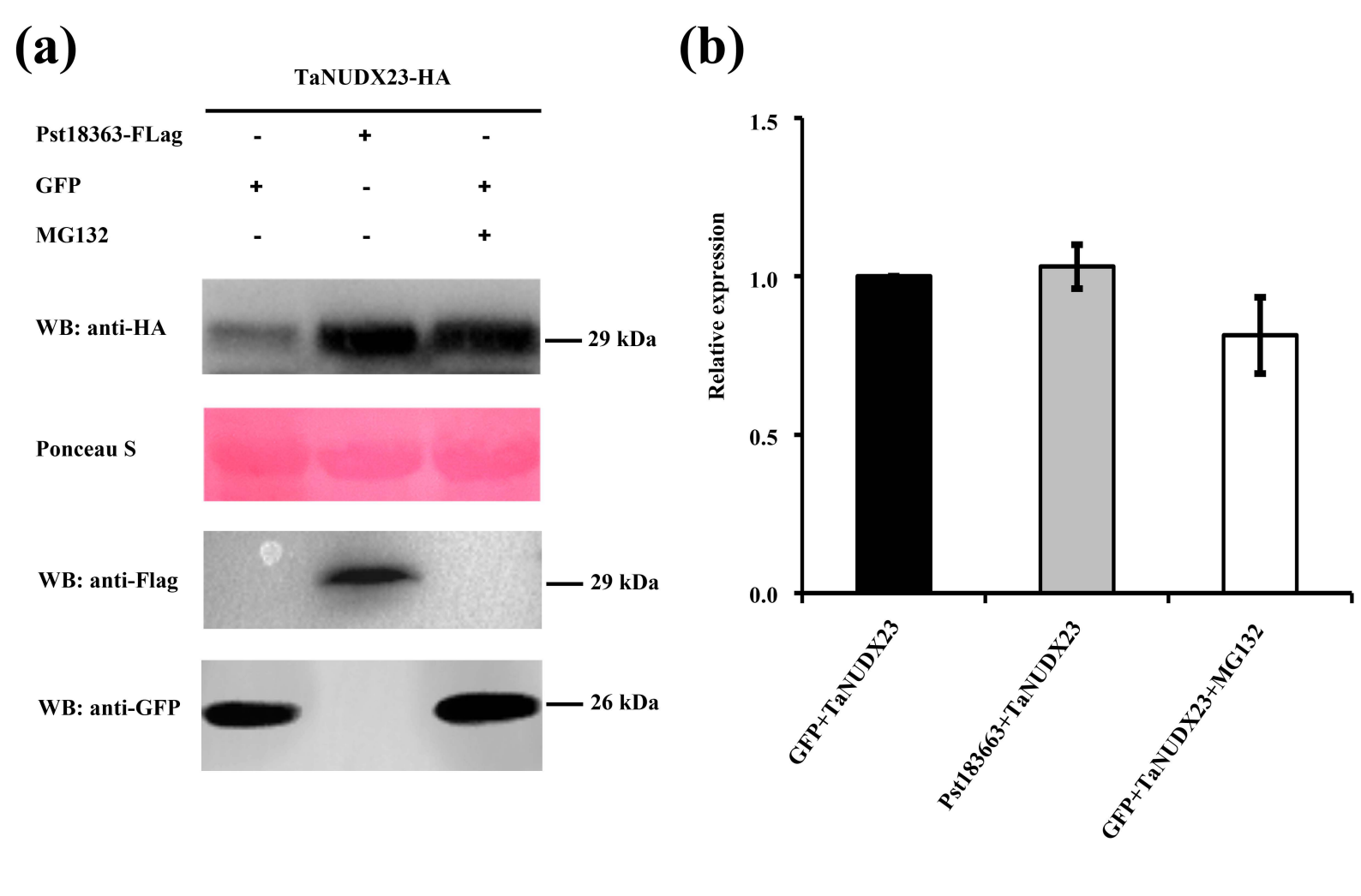
(a)
TaNUDX23-HA
Pst18363-FLag
GFP
MG132
WB: anti-HA
29 kDa
Ponceau S
WB: anti-Flag
29 kDa
WB: anti-GFP
26 kDa
(b)
Relative expression
1.5
1.0
0.5
0.0
GFP+TaNUDX23
Pst18363+TaNUDX23
GFP+TaNUDX23+MG132

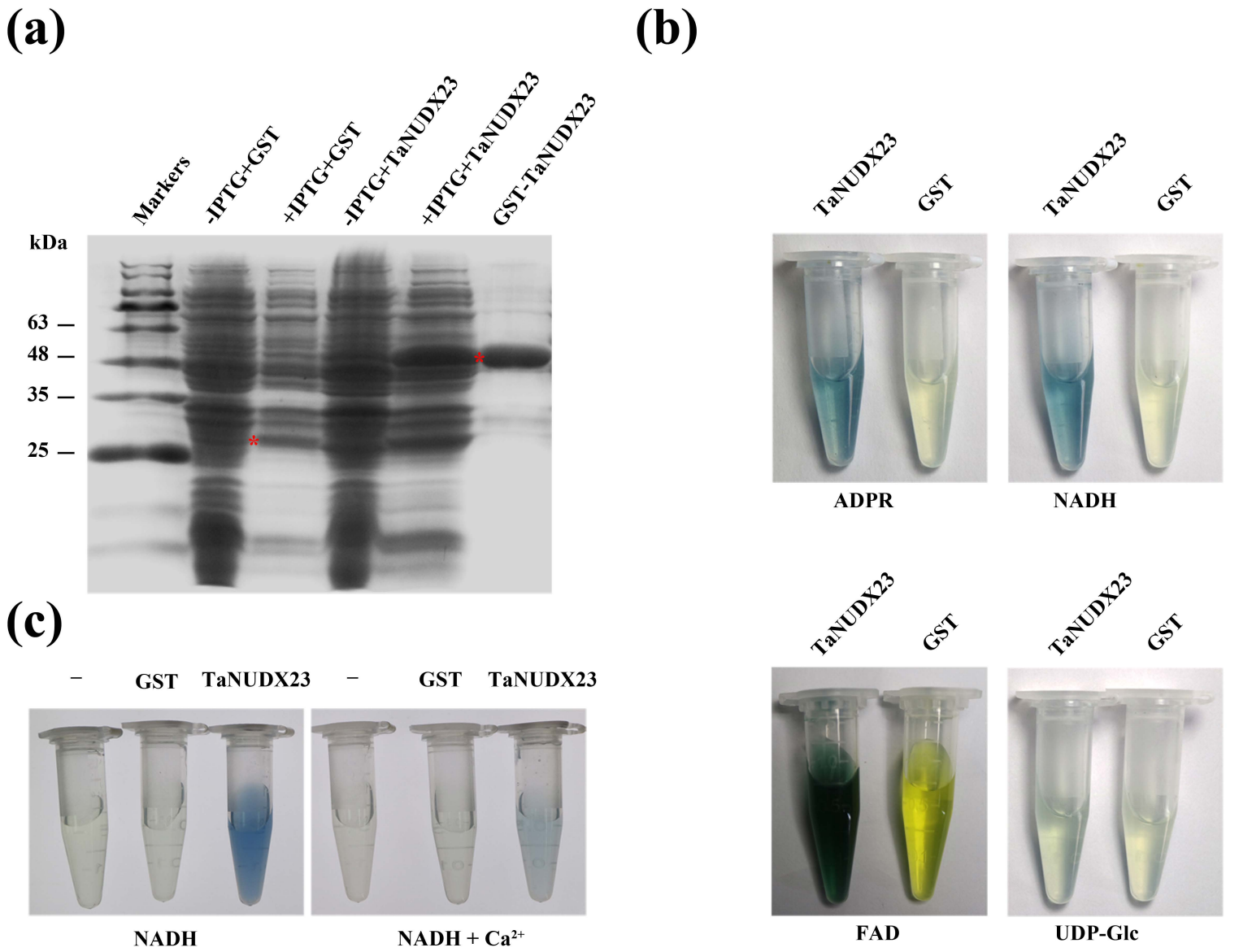
(a)
Markers
-IPTG+GST
+IPTG+GST
-IPTG+TaNUDX23
+IPTG+TaNUDX23
GST-TaNUDX23
kDa
63
48
35
25
(b)
TaNUDX23
GST
ADPR
NADH
FAD
UDP-Glc
(c)
–
GST
TaNUDX23
NADH
NADH + Ca2+

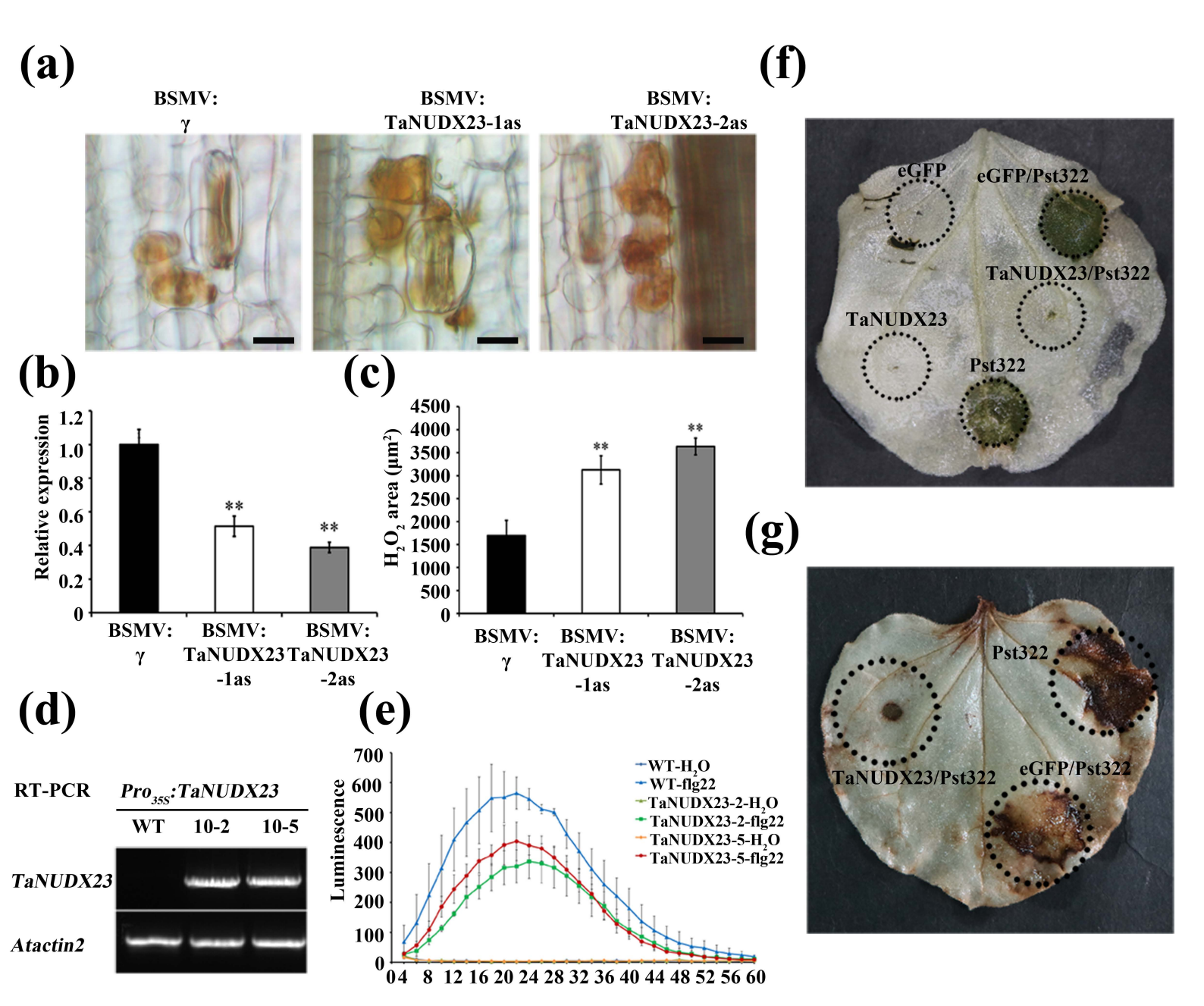
(a)
BSMV: γ
BSMV: TaNUDX23-1as
BSMV: TaNUDX23-2as
(b)
Relative expression
1.2
1.0
0.8
0.6
0.4
0.2
0
**
**
BSMV: γ
BSMV: TaNUDX23 -1as
BSMV: TaNUDX23 -2as
(c)
H2O2 area (μm2)
4500
4000
3500
3000
2500
2000
1500
1000
500
0
**
**
BSMV: γ
BSMV: TaNUDX23 -1as
BSMV: TaNUDX23 -2as
(d)
RT-PCR
Pro35S:TaNUDX23
WT
10-2
10-5
TaNUDX23
Atactin2
(e)
Luminescence
700
600
500
400
300
200
100
0
04 8 12 16 20 24 28 32 36 40 44 48 52 56 60
WT-H2O
WT-flg22
TaNUDX23-2-H2O
TaNUDX23-2-flg22
TaNUDX23-5-H2O
TaNUDX23-5-flg22
(f)
eGFP
eGFP/Pst322
TaNUDX23/Pst322
TaNUDX23
Pst322
(g)
Pst322
TaNUDX23/Pst322
eGFP/Pst322

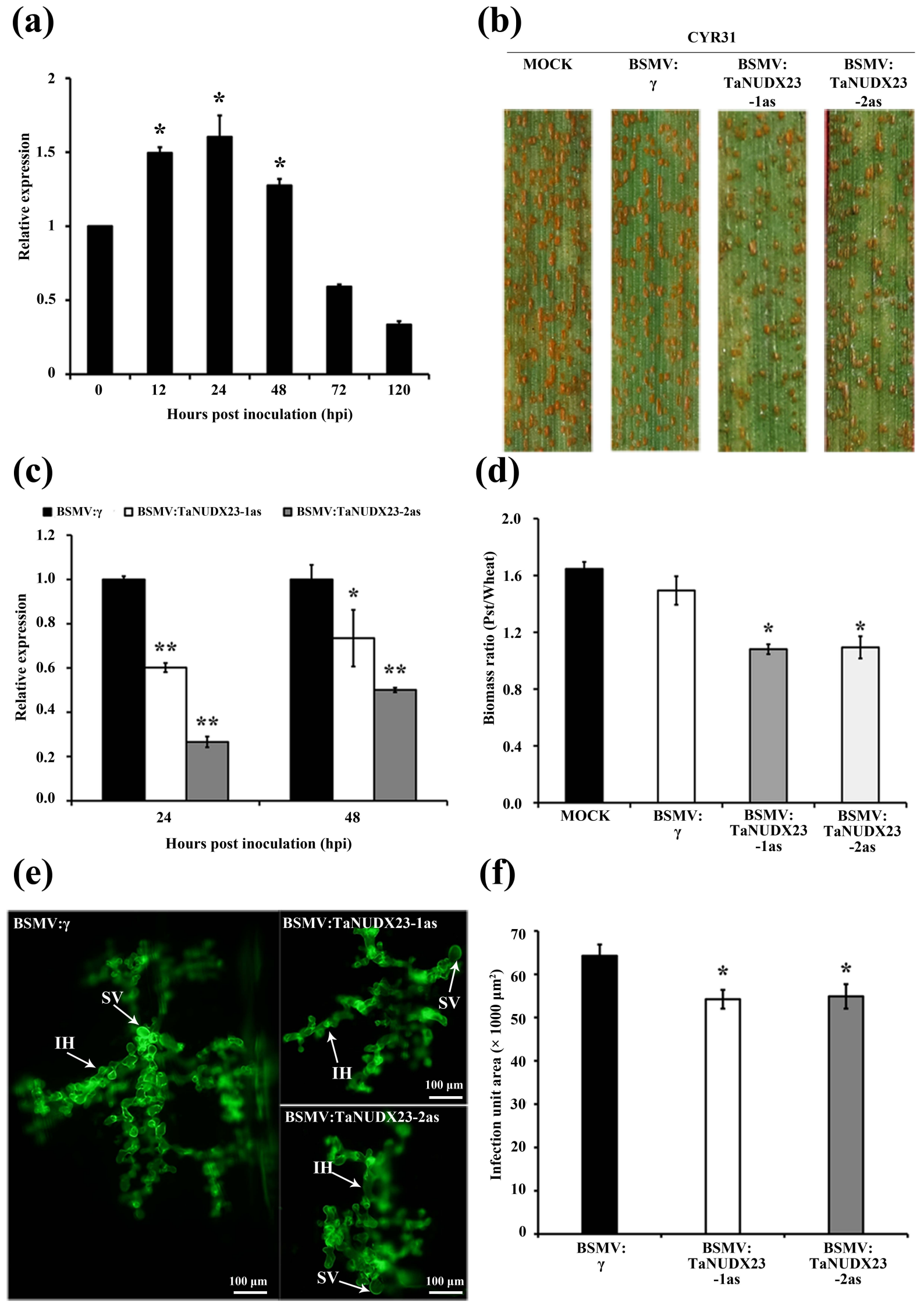
(a)
Relative expression
2
1.5
1
0.5
0
0
12
24
48
72
120
Hours post inoculation (hpi)
(b)
CYR31
MOCK
BSMV: γ
BSMV: TaNUDX23 -1as
BSMV: TaNUDX23 -2as
(c)
BSMV:γ
BSMV:TaNUDX23-1as
BSMV:TaNUDX23-2as
Relative expression
1.2
1.0
0.8
0.6
0.4
0.2
0.0
24
48
Hours post inoculation (hpi)
(d)
Biomass ratio (Pst/Wheat)
2.0
1.6
1.2
0.8
0.4
0.0
MOCK
BSMV: γ
BSMV: TaNUDX23 -1as
BSMV: TaNUDX23 -2as
(e)
BSMV:γ
SV
IH
100 μm
BSMV:TaNUDX23-1as
SV
IH
100 μm
BSMV:TaNUDX23-2as
IH
SV
100 μm
(f)
Infection unit area (× 1000 μm²)
70
60
50
40
30
20
10
0
BSMV: γ
BSMV: TaNUDX23 -1as
BSMV: TaNUDX23 -2as